A Digital Image Processing System for the Characterization of Frazil Ice

by Michael Paul Morris

A thesis submitted to the faculty of graduate studies in partial fulfillment of the requirements for the degree of

Master of Science

Department of Civil Engineering
University of Manitoba

Winnipeg, Manitoba, Canada

March, 2003

THE UNIVERSITY OF MANITOBA

FACULTY OF GRADUATE STUDIES

*****

COPYRIGHT PERMISSION PAGE

A DIGITAL IMAGE PROCESSING SYSTEM FOR THE CHARACTERIZATION OF FRAZIL ICE

BY

MICHAEL PAUL MORRIS

A Thesis/Practicum submitted to the Faculty of Graduate Studies of The University of Manitoba in partial fulfillment of the requirements of the degree of

Master of Science

Abstract

Frazil ice has a significant economical and social impact in northern regions around the world. The ability to predict the evolution and behavior of frazil ice based on environmental conditions, such as air temperature and water velocity, is an important step in minimizing its impacts on society. One method of advancing our understanding is through frazil ice research. An important aspect of frazil ice research is the ability to accurately detect and measure frazil ice. A number of instruments have been developed that can indirectly measure frazil ice concentration using electrical conductivity, laser Doppler velocimetry, acoustics, calorimetry, or time-domain reflectometry. Although frazil ice concentration is an important characteristic, a more detailed feature necessary for the advancement of frazil ice research is the particle size distribution. Photography is an excellent method of obtaining this information. Successful attempts have been made at using photography to capture images of frazil ice in the laboratory, but due to the labour intensive manual analysis, only a limited number of images could be captured and analyzed. In an attempt to improve the speed of image analysis and collect larger quantities of data, a digital image processing system was developed.

Frazil ice particles were produced in a counter-rotating flume housed in a large cold-room. Digital images of frazil ice were recorded under a cross-polarized light technique allowing the normally transparent ice crystals to be clearly distinguishable. A digital image processing system was developed to digitally manipulate and systematically analyze the images to extract the number, size, and location in the water column of every ice particle. This data could then be analyzed to reveal the temporal and spatial variation of frazil ice.

After the digital image processing algorithms were developed, a series of experiments were conducted and analyzed to test and validate the frazil ice generation and image processing procedures. The results indicated that the production and analysis of frazil ice particles were very reproducible. The results of the experiments were also compared to reveal the effects of air temperature and water velocity on the evolution of frazil ice.

Acknowledgements

Although my name is the only name on the title page of this thesis, I could not have come this far without the assistance and support from many people. I would like to take this opportunity to formally thank all of them.

I would like to thank my advisor, Dr. Doering for all his assistance, support and advice over the past few years. I enjoyed working with him and couldn't imagine doing my graduate degree with anyone else.

Thanks also go to my examining committee members, Bill Girling, Dr. Snelgrove, and Dr. Tachie for their questions and contribution to this thesis.

Thank you to my family who provided me with endless support and encouragement. Without your continuous support I know I would not have made it this far. Thanks!

Big thanks go out to Roy and my friends in the HRTF for making my pursuit of a higher education an enjoyable experience.

Thanks to the Natural Sciences and Engineering Research Council of Canada for honouring me with a PGS A Scholarship, to Manitoba Hydro for selecting me as a two time recipient of the prestigious Donald M. Stephens fellowship, to the Knowles family for providing me with the John Allen Knowles Memorial Scholarship, and to the Norrie family for awarding me the Duncan Norrie Memorial Scholarship.

Last, but definitely not least, I would like to thank Heather, for her never-ending patience, encouragement, and understanding.

Table of Contents

List of Figures

List of Tables

CHAPTER 1

Introduction

1.1 Background

As winter approaches and the air temperature drops below 0°C, river water will approach its freezing point. If a further drop in water temperature occurs in sufficiently turbulent open water, the water becomes supercooled and frazil ice begins to form. Frazil ice can have a significant impact on water resources infrastructure. For example, frazil ice can block water supply, reduce or shut down power generation at hydroelectric generating stations, interfere with shipping and navigation, damage or restrict the use of hydraulic structures, and constrict or block river cross sections causing flooding. Frazil ice can also attach itself to the riverbed, forming anchor ice, which changes the geometric and hydraulic properties of the flow. If anchor ice forms in the tailrace of a hydroelectric generating station increased staging may occur. This results in a reduction of the net operating head and a significant reduction in revenue. The economic and social costs of these ice related processes can be significant. Frazil and anchor ice problems have been documented at many hydroelectric generating stations operating in cold regions (Daly, 1991), including those in Manitoba (Girling and Groeneveld, 1999).

Studies of hydraulic impacts of frazil and anchor ice formation are limited (Shen, 1996). The ability to predict the effect that a parameter will have on the formation of ice is essential to the efficient operations of ravine activities in cold regions. Some parameters of interest include the river velocity, flow depth, river bed heat flux, bottom roughness, air temperature and the effect of ice cover. Frazil ice growth has been studied in both field (Yamazaki et al., 1996; Osterkamp et al., 1983) and lab

conditions (Michel, 1963; Carstens, 1966; Hanley and Michel, 1977; Tsang and Hanley, 1985). Results of these experiments indicate that the growth of frazil ice is influenced by many factors, but quantification of these effects has yet to be achieved.

The need to measure aspects and characteristics of frazil ice is a necessary first step in order to improve our understanding of frazil and anchor ice processes. However, direct measurement of frazil ice has proved to be difficult. White and Daly (1994) note:

> "Laboratory experiments have been a valuable tool for providing insight into many aspects of frazil ice formation, transport and interaction with sediment. The lack of practical and efficient ways to measure frazil ice concentrations in the laboratory or the field has been a problem. The even more desirable prospect of measuring the size distribution of frazil crystals seems a distant goal. The small size, nonspherical shape, and optical properties of frazil ice present daunting obstacles to be overcome in pursuit of this goal."

1.2 Frazil Ice Detection

An important element of frazil ice research is the ability to detect and measure the concentration of ice within a sample volume. Historically there have been a number of instruments developed for making such measurements with the majority being developed for laboratory environments.

Minerals present in natural water provide it with electrically conductive properties. As frazil ice crystals form, mineral impurities are ejected; as a result, frazil ice crystals are electrically non-conductive. By measuring the change in the electrical conductivity of water, it is possible to estimate the percentage of frazil ice present. Kristinsson (1970) was first to attempt to use the change in electrical conductivity to measure frazil ice concentration. Gilfilian et al. (1972) also used the change in conductivity (due to salt rejection) to estimate frazil ice concentration. Tsang (1985) used comparative resistance (i.e., conductivity) to improve instrument sensitivity and decrease sample volumes. Unfortunately, the bulk conductivity of ice/water depends on the shape and distribution of frazil particles, and accurate measurements require extensive calibration.

While electrical conductivity has been used to obtain field measurements of frazil ice concentration, numerous other methods have been used to measure frazil ice concentration in the laboratory. Schmidt and Glover (1975) used laser Doppler velocimetry, which counts particles passing through a control volume, to measure frazil ice concentrations. Their apparatus was capable of resolving concentrations down to 10^{-4}. Their approach requires the measurement of a constant that depends on the optical properties of the system and the shape of the frazil ice particles. These result in difficult calibration problems.

Hanley and Rao (1981) used acoustic properties to remotely sense the presence of frazil ice crystals. Optical instrumentation based on transmissivity and absorption were used by Pegau *et al.* (1996) to measure frazil ice concentration down to 10^{-3} and 10^{-2}, respectively. Both methods are capable of providing rapid in situ measurements of frazil concentration.

Yankielun and Gagnon (1999) used time-domain reflectometry (TDR) to detect the presence of frazil ice and provide estimates of the volume fraction of frazil ice in an immediate volume surrounding the probe. The method, which may be suitable for field monitoring of frazil ice, was tested in a laboratory setting. This method does not appear to be well suited to measure small concentrations of frazil ice.

Ford and Madsen (1986) developed a flow-through calorimeter but it lacked sufficient signal-to-noise to measure concentrations below 10^{-3}. The calorimetric approach of measuring the concentration of homogeneous, flowing mixtures of frazil ice was improved by Lever *et al.* (1992), who constructed a calorimeter capable of measuring concentrations as low as 10^{-4} to 10^{-5} with 1 to 3 minute sample times. Although Lever *et al.* (1992) developed their apparatus in laboratory setting, they believe that packaging for field deployment could be achieved.

The use of microscopy (Daly and Colbeck,1986) is well suited to measure relatively small concentrations of frazil ice. Daly and Colbeck's (1986) system discerned concentrations as low as 10^{-6} to 10^{-7} and was capable of detecting crystal sizes ranging from 30 μm to several millimeters. Unfortunately, this process required manual counting of individual frazil ice particles on each image. This labour intensive process limited the number of images that could be taken for a given experiment.

To conduct fundamental research directed towards characterizing the distribution and evolution of frazil ice size, shape, and concentration, the acquisition and analysis of in situ images of frazil ice appears to be one of the more promising methods. For this reason, a digital image processing system was selected for testing in the study described herein.

1.3 Research Objectives

The objective of this research is to develop a digital image processing system that can be used to examine and characterize the growth characteristics of frazil ice. The long term objectives are to use the processing system to improve the fundamental understanding of frazil ice processes in an attempt to mitigate frazil ice problems associated with Manitoba Hydro's hydroelectric system.

Chapter 2 details the unique research facility at the University of Manitoba used to study river ice processes. Chapter 3 presents the algorithms and digital manipulation techniques used to develop the Digital Image Processing System (DIPS). The results of a series of experiments are presented in chapter 4. The summary and recommendations for future work are given in chapter 5.

CHAPTER 2

Experimental Apparatus

2.1 Background

Experimental testing was conducted at the ice laboratory located in the University of Manitoba's Hydraulics Research and Testing Facility (HRTF). The ice laboratory consists of a cold room, a counter-rotating flume equipped with cameras, peripheral measuring instruments, and an image processor.

Ice can be observed from two different frames of reference, Eulerian and Lagrangian. Within a Eulerian frame of reference, observations of ice growth are made from a stationary position. For example, watching ice form on a rock while you are standing on the riverbank would be considered Eulerian. In an outdoor experimental environment, measurements of ice and flow characteristics as a function of time can be made at various stations along a riverbank. However, in a laboratory setting, a straight flume long enough to fully characterize the evolution of frazil ice is not practical since a flume several hundred meters long would be required. Several labs (Daly and Colbeck 1986; Michel 1963) however, use straight flumes to study frazil ice. In these labs water is re-circulated from the downstream end of the flume to an upstream head box. Unfortunately, the frazil ice particles are ripped apart as they are transported through the re-circulating pumps. This limits frazil ice evolution studies to the initial formation of ice particles only.

In a Lagrangian frame of reference, observations of an ice particle are made as the particle moves downstream. These observations are made from a station that floats alongside the ice particle. In a

laboratory setting, this type of observation could be made using a long flume, but like the Eulerian observations, the flume would have to be so long that it would not be feasible to construct. To overcome the complications associated with the long straight flume, a circular flume was employed as shown in Figure 2.1.

2.2 Counter-Rotating Flume

The circular flume in Figure 2.1 consists of a circular channel supported underneath by a turntable. The bottom of the channel is separate from the channel walls and is supported by an independent overhead structure. This allows the bottom and the walls of the channel to rotate independently, in opposite directions. Figure 2.2 shows a schematic of the various structural components of the flume that allow for the counter-rotating effect. The flume channel is 0.2 m wide, 0.35 m deep and has a centerline diameter of 1.2 m.

The bottom of the channel is lined with six plastic plates embedded with a uniform layer of gravel, to simulate the bed material roughness in a river. Exchanging bedplates with those that have a different gravel size changes the roughness of the flume. This allows control of the hydraulic characteristics of the water and greater flexibility when choosing experimental variables. Figure 2.3 shows three plates with different gravel sizes. The blue coloring on and around the gravel is epoxy used to hold the gravel in place.

Simulation of straight channel flow using a rotating body of water produces undesirable centrifugal forces. These forces may change the floc size and concentration of frazil and lead to uneven lateral distribution of ice flocs. Additionally, unrealistic water surface profiles are also encountered. Figure 2.4 compares the water surface profile produced by straight channel flow and a rotating body of water. In order to overcome these centrifugal forces, the sides of the flume rotate in one direction while the bottom portion rotates in the opposite direction, hence the name, counter-rotating flume. Two tachometers, mounted on motors controlling the bed and walls, are used to measure the rotation rates. These rates are adjusted until the shear stress generated from the sides is equal to the shear stress acting on the bottom. This creates a stationary water column, relative to an observer standing beside the flume, eliminating the centrifugal forces. Figure 2.5 shows the flow meter used to determine the shear force balance. The flow meter was placed at 60% of the water depth and the bed

speed was set at a constant value. The wall speed was then adjusted until its angular velocity matched the water velocity as measured by the probe. When this condition was satisfied, the water column was deemed to be stationary. This process was repeated at various bed speeds to create calibration curves (Figure 2.6). A unique curve is required for each bed plate gravel size and water depth combination.

The water velocity used to describe each experiment is calculated from a frame of reference relative to the bed, since the actual water velocity is zero. The effective water velocity is calculated by converting the rotational rate of the bed, measured in RPM (revolutions per minute), to its angular velocity. This conversion can be made using the following equation

$$V_e = (\pi d)x(V_b)$$
$$=(3.14*1.20\ [m])x(V_b\ [RPM])$$
$$=3.77\ V_b\ [m/minute]$$
$$=6.28\ V_b\ [cm/s]$$

where V_e = Effective water velocity [cm/s]
d = Centerline diameter of the flume (1.2 m)
V_b = Velocity of the bed [RPM]

The velocity profile generated in the flume is realistic when viewed from a frame of reference relative to the bed. The maximum velocity occurs at the surface while the velocity decreases inversely with depth until a velocity of zero at the boundary layer over the bed is attained (Figure 2.7 (a)). This velocity profile occurs in a natural stream. However, relative to an observer standing beside the flume, the velocity profile produced by the flume is somewhat reversed. The velocity at the surface is zero while the maximum velocity occurs at the bed (Figure 2.7 (b)).

This reversal of the velocity profile may alter the natural interaction at the water/air interface. Since the cooling force of the water is driven by the heat exchange at this interface, changing the characteristics of the water/air interface may have an effect on the cooling rate of the water. The quiescent nature of the surface produced in the flume may alter these characteristics and change the cooling rate for a given air temperature. Therefore, the experiments are described using their cooling rates as well as the air temperature.

A ground heat flux from the riverbed is simulated by circulating warm air in a duct just under the gravel-embedded bed plates. The duct is equipped with a heater and fan to maintain a near constant temperature of 5°C. Although this air temperature may seem warm, it is separated from the water by a 5 cm thick layer of UHMW (Ultra High Molecular Weight) plastic, which acts as an insulator. Thermometers embedded in the UHMW plastic indicate that the temperature of the plastic, just below the embedded gravel, is 0°C. To prevent the sidewalls of the flume from icing, warm air is circulated in ducts surrounding the flume walls. A heater lamp connected to a controller is activated whenever the air temperature in these ducts falls below +2°C. The warm air is circulated through the wall ducts with a fan. The temperature in all three ducts (inner, outer and bottom) is monitored using an array of RTDs . An RTD or Resistance Temperature Detector is a device that indicates temperature by measuring the change in resistance of a material.

The water temperature is measured using a 4 wire RTD (Omega PR-11-3-100-1/8-6-E). The probe is inserted into the flow from the side (Figure 2.8) to prevent any interaction between the water/air interface that would occur if the probe was inserted from the surface. The temperature/voltage signal from the RTD ranges from 0 to 10 volts for a temperature ranging from –1°C to +2°C.

The location of the camera in its rotation around the flume is an important consideration in the image processing procedures. The rotational location is recorded using an LED (Light Emitting Diode) (Figure 2.9) and switch. A switch, mounted on the underside of the rotating flume, is triggered once every rotation to activate an LED for 1 sec. The LED is positioned inside the camera box such that it can be seen on the bottom left corner of each image. By observing when the LED is turned on, the rotational position of the cameras can be determined. Figure 2.10 shows two images, one with the LED on and the other with the LED off.

2.3 Coldroom

The counter-rotating flume is located in a cold room (Figure 2.11) 4.3 m wide, 4.3 m deep and 2.7 m high. The chamber is constructed of 100 mm thick Norbec insulated panels with an insulation-value of R30. It is equipped with two Blanchard Ness outdoor air cooled condensing units, each with a capacity of 48 000 BTU's. Each condensing unit is coupled with a Blanchard Ness low silhouette evaporator coil via a Sporlan CDS-8 step motor evaporator control valve. This dual compressor system permits "infinite" experiments to be conducted. By cycling the compressors, one

compressor/evaporator system is allowed to defrost while the other maintains the temperature. The temperature of the coldroom is regulated with an Omron E5GN temperature controller mounted outside the coldroom. The temperature control system is also equipped with an IEEE-485 port to allow full computer control and monitoring of the PID controlled compressor systems. The temperature limit of the coldroom is -30°C with a variation of ± 0.1°C.

2.4 Image Recording Equipment

The flume is equipped with two cameras located in a box on the side of the flume (Figure 2.12) that record the frazil ice as it forms and evolves. Figure 2.1 shows a technician adjusting the cameras in the camera box. Each camera transmits its signal to a monitor located just outside the coldroom. The first camera is a Panasonic color camera that records a wide-angle view of the water column. The signal from this camera is not used in the analysis process; rather it is used to observe the progress of the experiments on a monitor located outside the coldroom. The second camera (Figure 2.13) is a Sentech STC-1100 black and white progressive scan camera with a field of view of 16.5 cm (horizontal) by 12 cm (vertical). The analog signal from this camera is sent to a DIPIX FPG-44 Power Grabber board installed in a computer where the signal is converted to a digital image consisting of 640x480 pixels with 256 shades of grey. This digital image is then recorded directly to a computer hard drive. The image recording system can capture and record 15 frames per second.

The video recordings are made using cross-polarized light as illustrated in Figure 2.14. Located inside the center of the flume, opposite the cameras, is a light source and a polarizing sheet (Polarizer 1). Each camera lens is also fitted with a polarizer (Polarizer 2) that is positioned so that the optic sills are perpendicular to the optic sills of the first polarizing sheet. This creates a cross-polarizing condition. The first polarizing sheet filters light oscillations perpendicular to its optic sills, while the polarizing sheet on the lenses filters the light in the other principle direction, preventing any light entering the camera directly from the light source. The only way light can enter the camera is after it has passed through a particle of ice. Ice particles regenerate oscillations that were filtered out by the first polarizing sheet. This allows the normally transparent ice crystals to be seen distinctly by the camera.

The camera position is set so that the surface of the water is a few millimeters above the camera's field of view. Due to the cross-polarized lighting conditions, the interface of the water surface and the air regenerate some of the light oscillations that were just filtered out by the polarizing sheet (Polarizer 1). These redeveloped oscillations cause the water surface to appear very bright. Since ice particles also appear very bright, the system used to analyze the images falsely identifies the surface as ice. Therefore "moving" the surface out of view of the camera avoids this problem.

2.5 Peripheral Data Acquisition

A Keithley Metrabyte DAS-1600 data acquisition board was used to record water temperature, outer, inner and bottom cavity temperatures, and rotation rates for the bed and walls. Data was sampled at 2 Hz using LABTECH NOTEBOOK version 10.

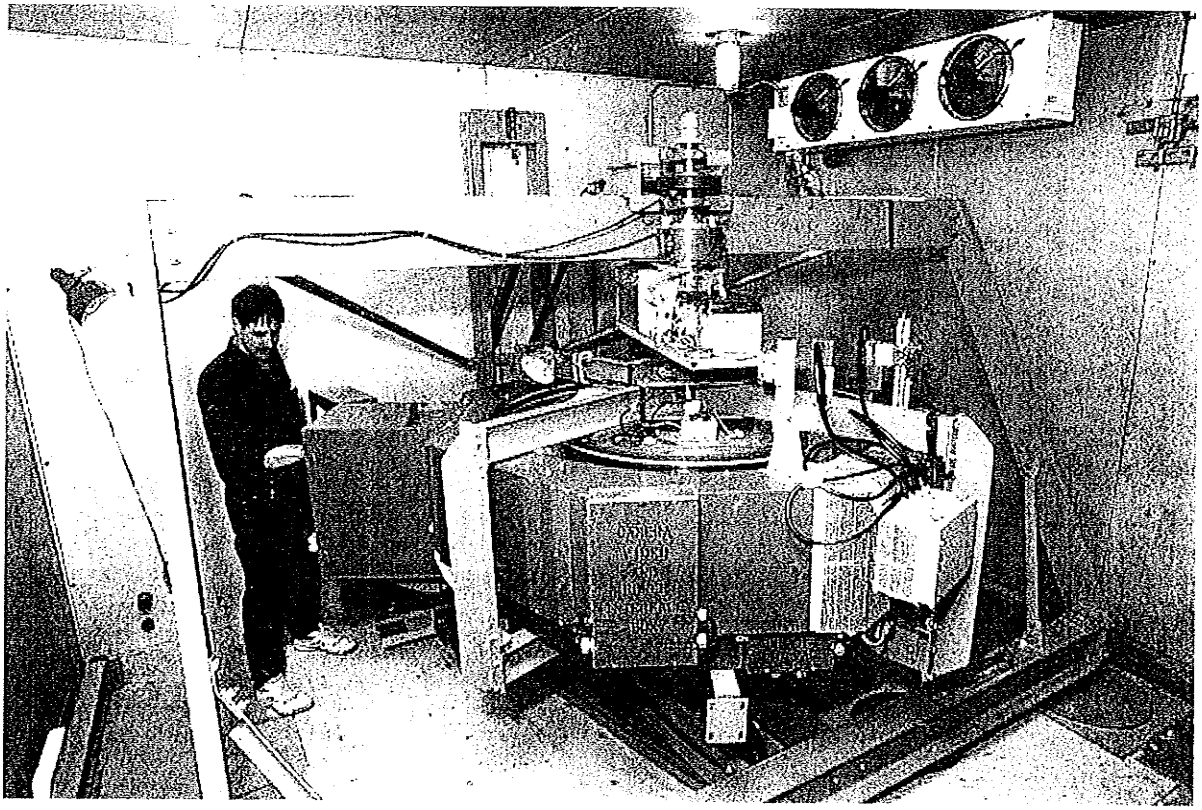

Figure 2.1. Counter-rotating ice flume.

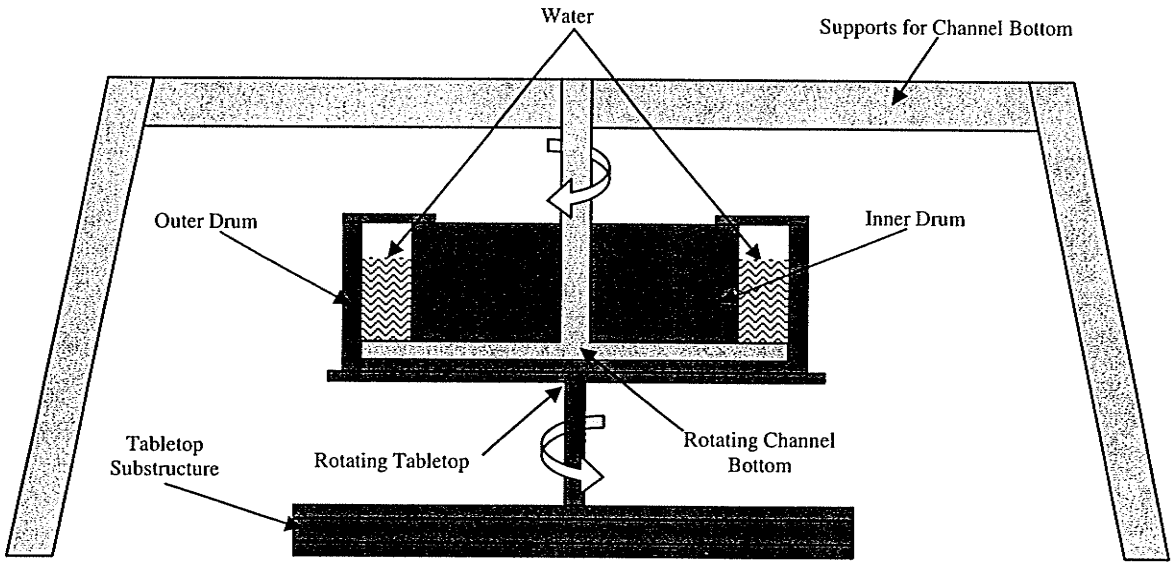

Figure 2.2. Schematic of the various structural components of the counter-rotating flume.

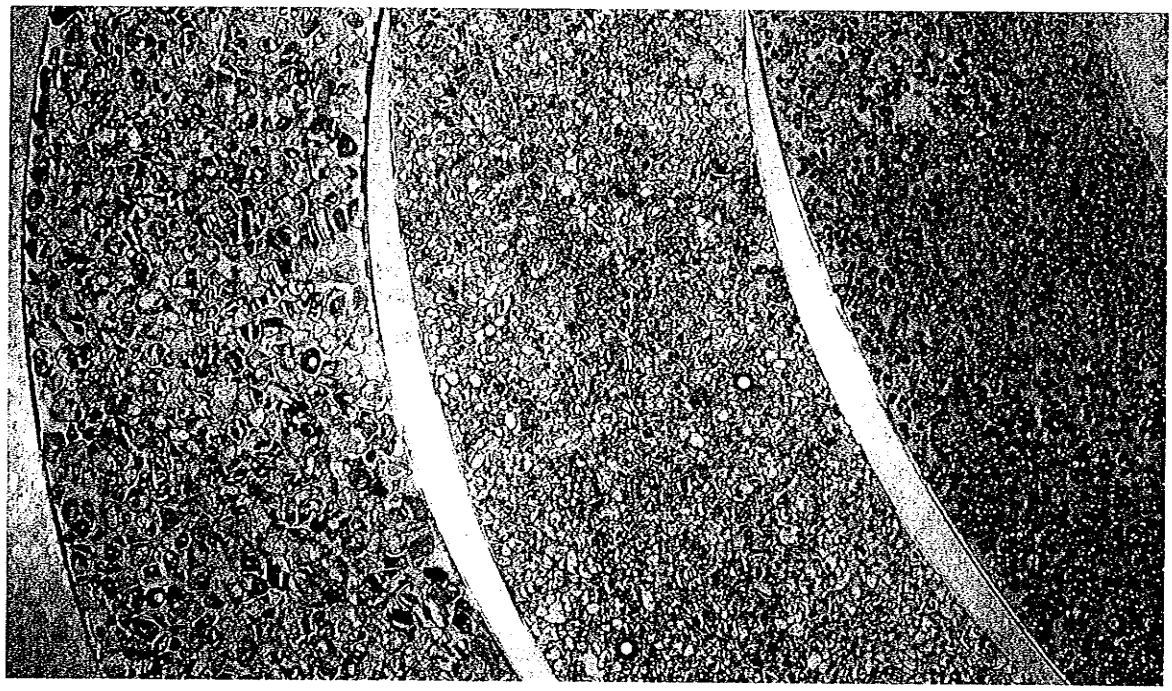

Figure 2.3. Three bedplates with different sizes of embedded gravel.

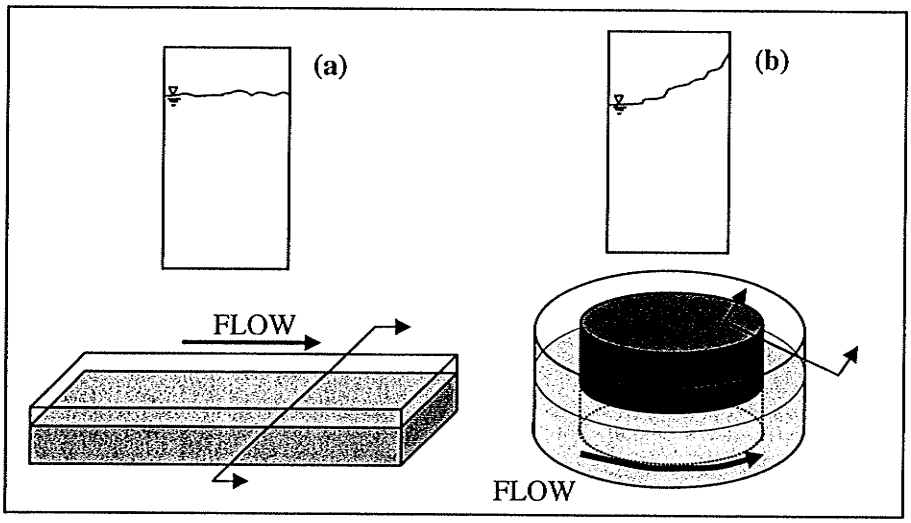

Figure 2.4. The water surface profile produced by **(a)** straight channel flow and **(b)** a rotating body of water.

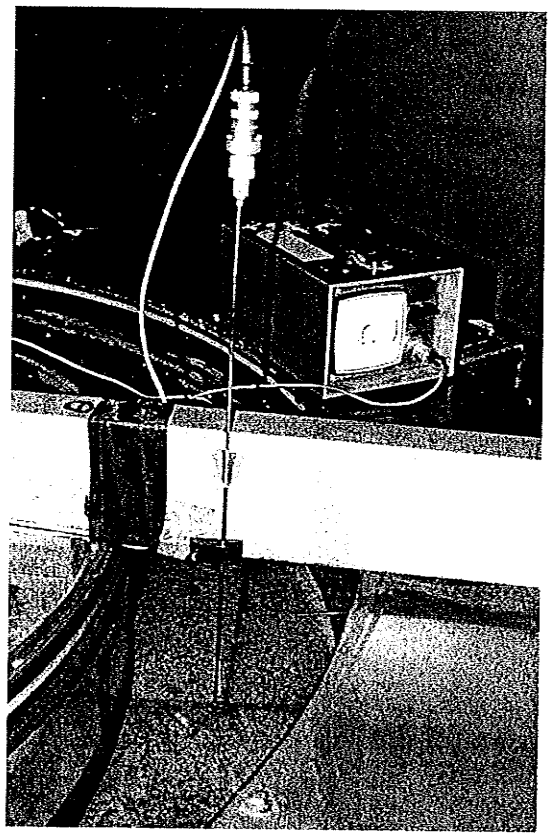

Figure 2.5. Flow meter used in wall and bed rotation rate calibration procedure.

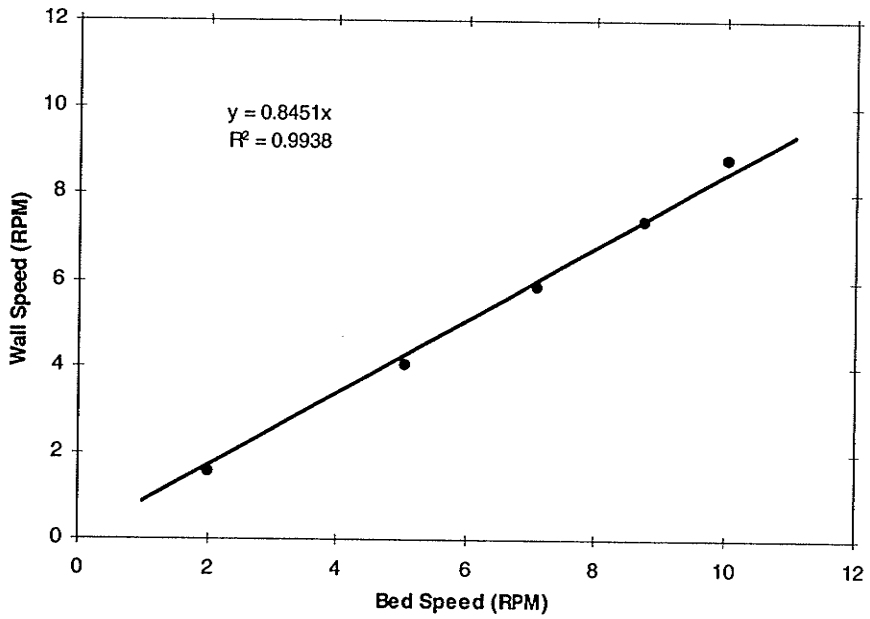

Figure 2.6. Calibration curve for wall and bed speed balance for a bed roughness diameter of 5mm and water depth of 15 cm.

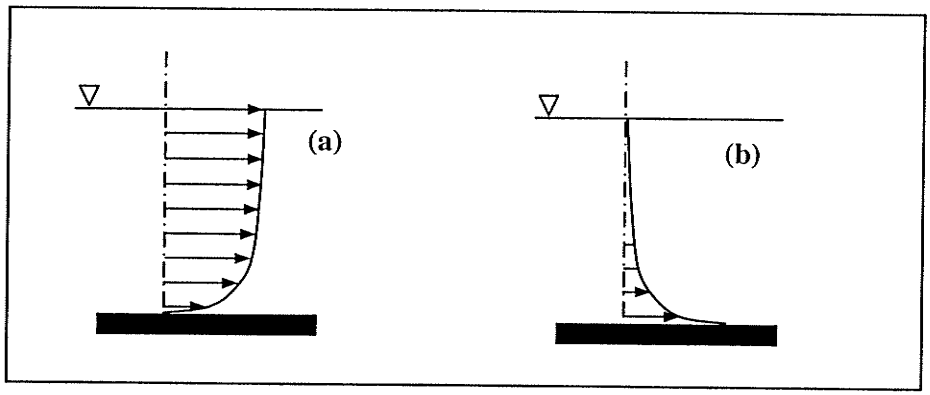

Figure 2.7. Velocity profile generated in **(a)** open channel flow and **(b)** in the counter-rotating flume.

Figure 2.8. The RTD submerged in the water from the side of the flume.

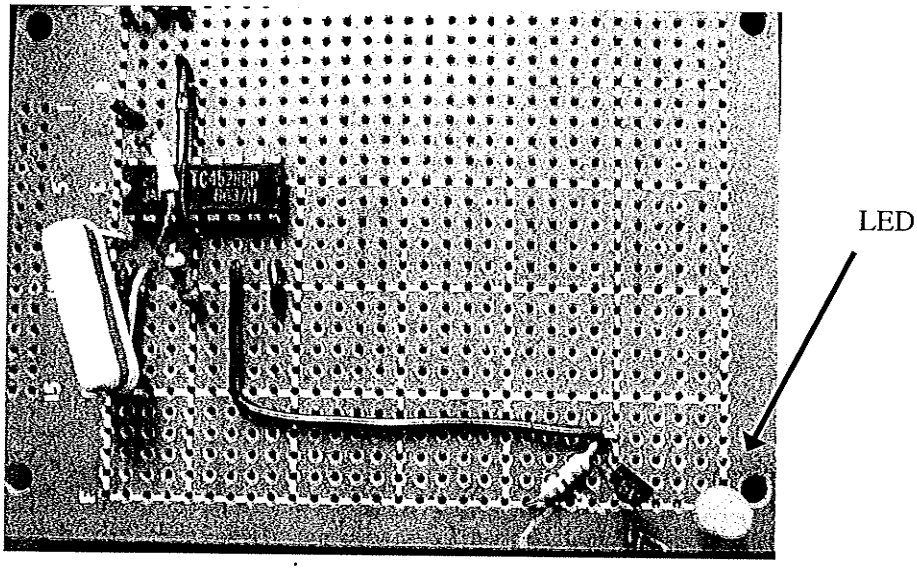

Figure 2.9. LED and circuit board.

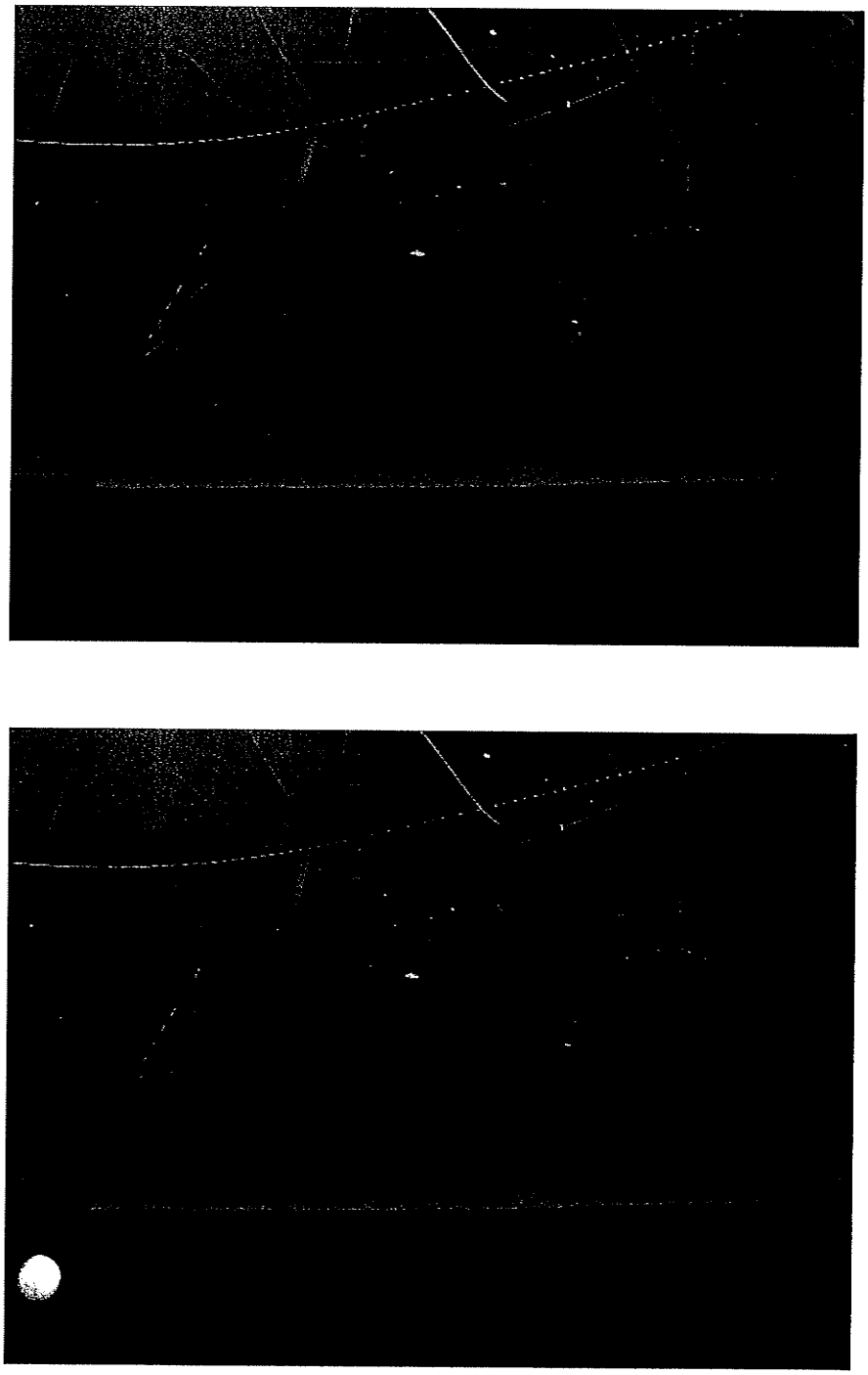

Figure 2.10. Image with **(a)** the LED OFF and **(b)** the LED ON.

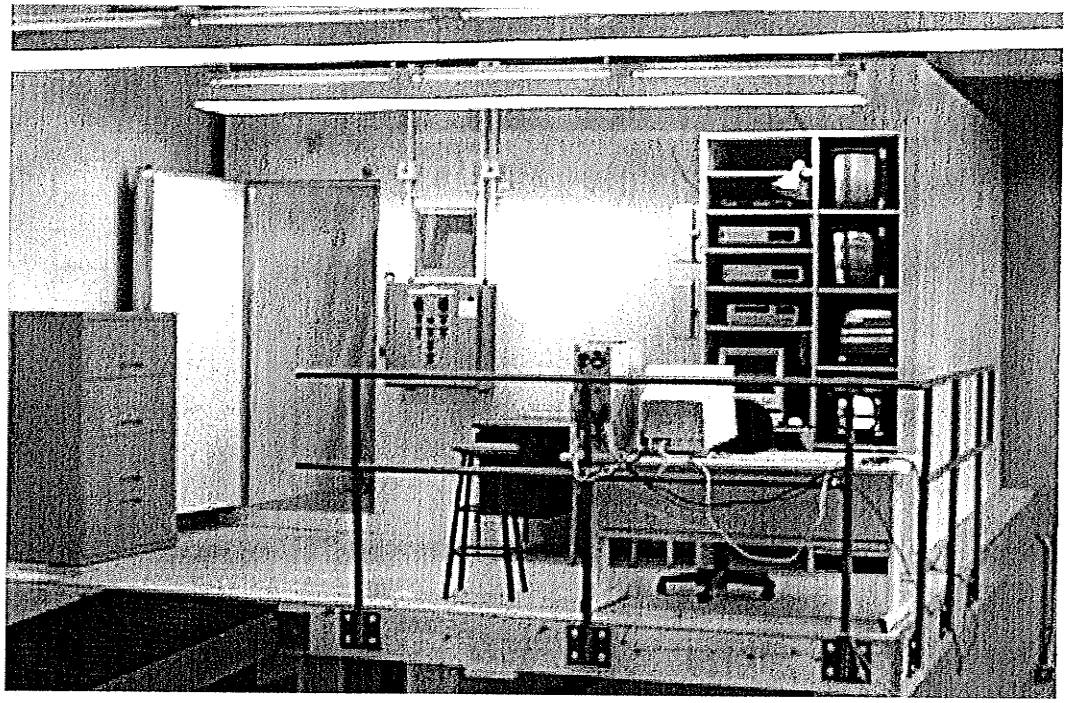

Figure 2.11. HRTF's cold room.

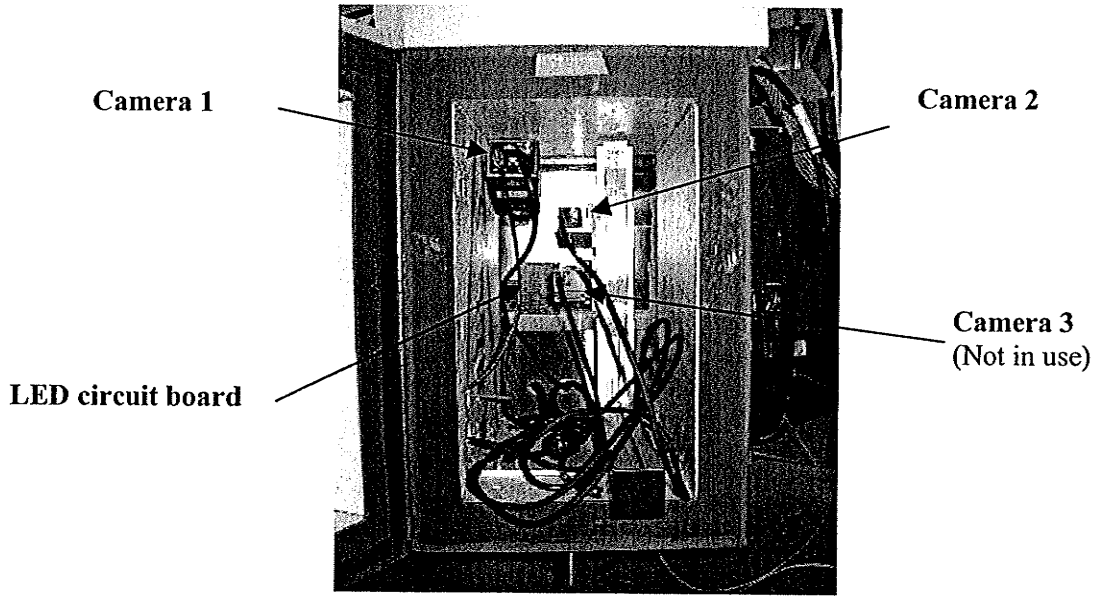

Figure 2.12. Cameras and LED housed in the camera box.

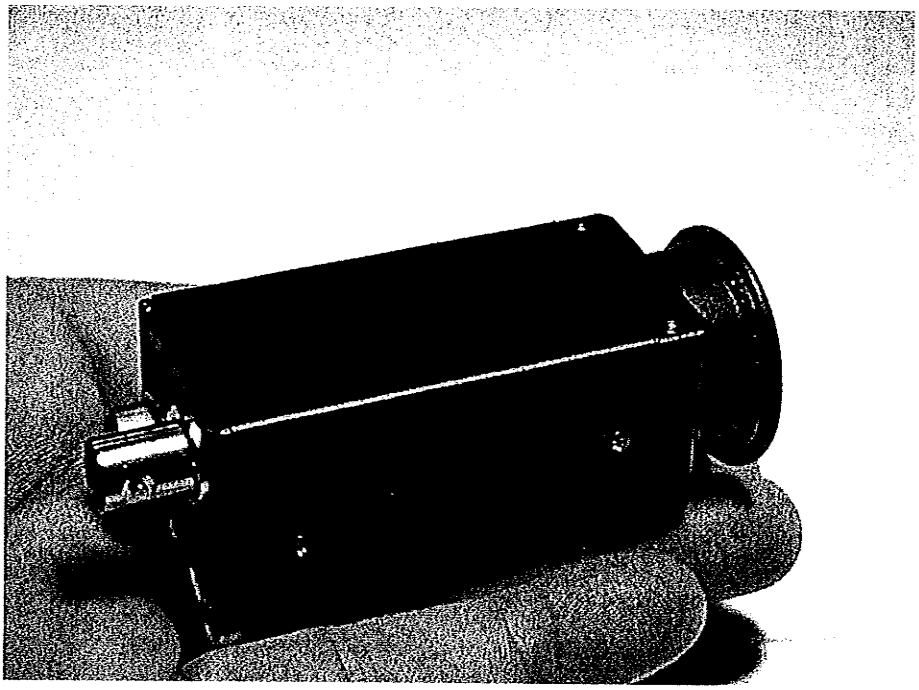

Figure 2.13. Camera 2, a Sentech STC-1100. (From Sentech User Manual)

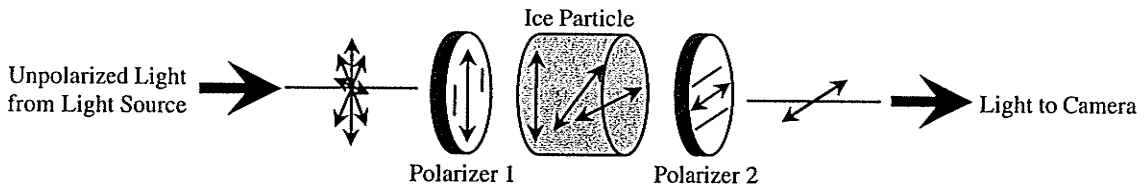

Figure 2.14. Cross-polarized light scheme.

CHAPTER 3

Digital Image Processing System

In order to extract information about the evolution of frazil ice particles within the counter-rotating ice flume, a digital image processing system was developed. The processing system includes image acquisition, image enhancement, particle recognition and counting, and data exhibition. First, the progressive scan camera, frame grabber and computer collect and store images from the flume directly on the hard drive. After all the images are collected, they are enhanced and analyzed to extract the size and location of each individual ice particle within each image. This information can then be used to study the change in size and spatial distribution of frazil ice over the course of each experiment. The programs and processes developed to capture and analyze the images containing frazil ice are discussed in this chapter.

3.1 Image Acquisition

The Dipix frame grabber and Sentech camera are capable of capturing up to 15 frames per second. The continuous collection of 15 frames per second throughout the entire experiment, which typically runs for 1-2 hours, would result in an enormous amount of data. A one hour experiment, continuously collecting 15 frames per second, would yield 54 000 images requiring 16.2GB of storage space. To reduce the quantity of information to a manageable size, a program written in C++ was developed to communicate with the frame grabber, camera and computer in order to coordinate

the image acquisition process. Instead of an uninterrupted acquisition process, a specified number of images are captured at regular intervals at an appropriate grab rate.

At the start of each experiment, the digital image capturing program prompts the user for four variables: "Grab Rate", "Time Between Cycles", "Frames per Cycle", and "Save Images to". Figure 3.1 shows a screen shot of the input prompt for the image-capturing program. The "Grab Rate" refers to the speed at which the images are collected. Typical video camera captures between 24-30 frames every second. Hardware used in this research is only capable of capturing a maximum of 15 frames per second. The images gathered are not collected on a continuous basis; rather they are collected in bursts. The time between the collection bursts is referred to as the "Time Between Cycles". The number of images collected during each burst is referred to as "Frames per Cycle" and the directory on the computer where the images are saved is entered in the "Save Images to" variable.

A typical experiment uses the following protocol: 50 frames grabbed per cycle acquired at a rate of 3 frames per second; this process is repeated every 60 seconds. Figure 3.2 illustrates an example of the image collection schedule using the typical input parameters. At the start of every cycle, the program will start collecting frames at the specified grab rate, until the specified number of images has been collected. The computer waits until the start of the next cycle and then repeats the grab process.

A grab rate of 3 seconds is typically used to prevent any substantial overlap of the images. If the grab rate was set too high, the sequentially acquired images would overlap and contain the same particle of ice. This would skew the end results since some particles would be counted twice in the image processing system. A substantial overlap would also increase the number of images needed to completely record the water column of the entire flume.

The transfer of images from the camera directly onto the hard drive would limit the speed of image capture. As a result, the images captured during each cycle are initially stored on the RAM of the computer. After one complete cycle of images have been collected and stored in RAM memory, the images are then transferred to the hard drive. This intermediate storage of the images in RAM and the subsequent transfer to the hard drive limits the number of images that can be grabbed for a specific grab rate and cycle length. For example, if the image acquisition program was set to grab 100 frames at 1 frame per second, the total grab time would be 100 seconds. Since it takes approximately 20 seconds to transfer 100 images from RAM to the hard drive, the cycle length could not be less than 120 seconds (100 seconds to capture + 20 seconds to transfer). Also, there is a

limited capacity of RAM storage. If the image acquisition program were set to grab 10 000 frames before they were transferred to the hard drive, the computer would run out of RAM and the images would be lost or the computer may crash. The computer used during this research could hold up to 400 images in RAM, but this value could be increased by increasing RAM size.

3.2 Digital Image Manipulation

The digital images collected are grey scaled, TIFF (**T**agged **I**mage **F**ile **F**ormat) images with a resolution of 640x480 pixels. Each image is actually a 640x480 matrix with each cell value ranging from 0 to 255, where 0 represents black, 255 represents white and all the numbers in between are shades of grey (higher numbers are brighter). Since each image is simply a matrix of numbers, it can easily be manipulated with mathematical software. The software used in this research was MATLAB® Release 12 equipped with the image processing and signal processing toolboxes.

Object and pattern recognition appear quite simple when performed by the human eye and brain, but as simple as they may seem, it is very difficult to reproduce the speed and accuracy on a computer. Humans rely on the eye to successfully identify certain boundaries or edges of an object before that object can be identified (Burton, 1995). These edges are the most important perceptual feature of an object because they define where the object begins and ends relative to the background and other objects. For images used in this research, edges are defined by changes in local intensity, which can be seen as a sharp division in brightness. Figure 3.3 shows an image that contains several particles of frazil ice that are distinguished from the background by their difference in brightness.

Since each experiment has several thousand images to process, it would be virtually impossible to manually observe each image and count the number, size and location of every particle of ice. Instead, a digital image processing system was developed to automatically analyze each image and recognize each particle of ice based on its brightness.

3.2.1 Reference Image Creation

The first step in the processing system is the removal of the background "noise" from each image. Inherent in each image are small scratches from the Plexiglas and non-uniform lighting conditions. It is important to remove these irregularities before the processing system begins its particle recognition process, since they may be misinterpreted as a particle. This removal process begins by comparing an ice image to a reference image. The term "ice image" refers to an image taken during an experiment that contains particles of frazil ice, while "reference image" refers to an image captured prior to any ice formation. By comparing these two images, individual particles can be recognized by assuming any difference between the images is attributed to frazil ice.

There are actually multiple reference images. As the flume rotates, it causes the Plexiglas separating the water from the cameras to flex. The degree of flex is very small and is dependent on the rotational position of the flume. For example, at Point A in Figure 3.4, the flex is at its maximum, but as the flume rotates, the flex gradually decreases to a minimum at Point B, 180° from Point A, and then continues to increase until the flex is at its maximum again at Point A. The source of the flex in the Plexiglas is believed to be a very small misalignment of the structure responsible for the movement of the flume walls. The flex has no structural implications due to its small magnitude, but it does significantly affect the optical properties of the Plexiglas.

As explained earlier, the camera is set up using a cross-polarized lighting scheme. As the Plexiglas flexes, the optical properties are changed, causing some of the previously filtered light oscillations to be regenerated. These newly generated oscillations pass through the polarizing filter on the camera, appearing as bright areas on the images. The change in brightness caused by the flexing Plexiglas is not uniform over the entire image; rather it is concentrated in the upper left corner of the images. Figure 3.5 shows the average brightness of the upper left quadrant for a series of images collected as the camera rotated around the flume. The average brightness refers to the average value or intensity of every pixel in the image matrix. The brightness ranges from a maximum of 81 to a minimum of 58. Since every pixel on the image can only vary from 0 to 255, this brightness shift of 23 units represents almost 10% of the available intensity range. This magnitude of shifting brightness has a significant effect on the particle recognition process.

It is quite clear from Figure 3.5 that the change in brightness occurs in an intermittent manner with a period of 18 images. The period of 18 images corresponds to the number of images taken during 1 complete revolution of the flume. The images used to create this figure were captured at a rate of 3 images per second while the walls were rotating at a speed of 10 RPM or 6 seconds/revolution. Therefore, each 6-second revolution captures 18 images, which corresponds to the period measured from Figure 3.5. This confirms that the change in brightness occurs in the same location for every rotation.

In the early development of this processing system, before the flexing Plexiglas quandary was discovered, only one reference image was used. This reference image was comprised of an average of 50 images taken from various locations around the flume. This single, averaged reference image had an average brightness, when compared to images captured from different locations of the flume. This produced skewed results since the particle recognition system compares the brightness of the ice images to the brightness of the reference image. If the ice image was taken near the brightest location at Point A, the average brightness of that image would be higher then the single reference image. This situation would cause the particle recognition process to falsely identify particles. Likewise, if the ice image was taken near Point B, its brightness would be lower than the brightness of the single reference image, causing ice particles to be missed in the recognition process. To overcome this changing brightness problem, several reference images are created at various rotational positions to represent the full circumference of the flume.

The flume was not equipped with any device that recorded the exact location of the flume in its rotation. This became a problem when trying to line up the ice image with its correct reference image, which was taken at the same location in the flume. This problem was rectified using an LED and switch described earlier. By analyzing the images and looking for the LED, the relative position of the flume was determined.

At the start of the experiment, after the rotation rates of the walls and bottom have been set but before any ice begins to form, 400 images were captured at the same rate as the experiment. These images will be averaged to create the reference images. If the grab rate is set at 3 frames per second and the rotation rate of the walls is set at 10 RPM (6 seconds per revolution), each revolution of the flume will capture 18 images. Therefore, for this set of parameters, the flume is represented by a collection of 18 reference images called the reference image set. Since each revolution only captures 18 images,

the 400 images will be collected over more than 22 revolutions of the flume. The images from each revolution are averaged together in a manner described below.

The number of images in the reference image set was not actually calculated using the capture rate or RPM setting of the walls. Rather, it was determined by analyzing the LED imprint on each image. The LED is in a fixed position on all of the images, in the bottom left-hand corner. By monitoring the brightness in this small corner, it was possible to see when the LED was on or off. Figure 3.6 shows the average value of the pixels (brightness) of a small box in the bottom left-hand corner for a portion of the sequence of 400 images taken before the experiment. This figure clearly shows when the LED is energized. By measuring the period of this "wave", the number of images captured per revolution was determined. It is this value that was used to establish the total number of images in the reference image set.

Once the number of images in the reference image set had been determined, the actual images were then created. Averaging all the images from the set of 400 in which the first occurrence of the LED appears in each "wave", forms the first image in the reference image set. From Figure 3.6 this would include images marked by the square (■). The second image in the reference image set would be an average of all the images directly following the first appearance of the LED (marked with an asterisk (*) in Figure 3.6). This process is repeated until the complete reference image set has been created. The last image in the reference image set will be the image directly before the first appearance of the LED. These images are marked by a triangle (▲) in Figure 3.6.

The end product is a file composed of the same number of images as the period, with the first image representing the first occurrence of the LED. Figure 3.7 shows the LED signature of the reference image set. Since the LED always turns on at the same position in the flume's rotation, each image in the reference image set represents a specific location around the flume, see Figure 3.8. The whole process of creating the reference image set is completed only once for each experiment.

3.2.2 Position Vector

Once the reference image set has been created and all the ice images have been collected, the actual image processing begins. For each cycle of images, it is important to align the ice images with the correct reference image. The ice image and reference image are aligned when both images were

captured at the same rotational position. The LED is used again to determine the rotational location of the flume when each ice image was captured. By analyzing the bottom left corner of the ice images for one cycle, typically 50 images, the pattern of LED lighting can be clearly determined. Figure 3.9 illustrates the lighting of the LED for one complete cycle of ice images.

The next step is to identify the ice image where the first excitation of the LED occurs. This image would be labeled with a "1" because it corresponds to the first image in the reference image set. The image following image "1" would be labeled with a "2" because it corresponds with the second image in the reference image set. This labeling process continues in the forward direction until an ice image is labeled with the number that corresponds with the total number of images in the reference image set (in Figure 3.9, this number is 18, which also represents the period). The labeling process then begins again by labeling the next image with a "1" and the process of labeling continues in the forward direction until the last ice image is labeled (in Figure 3.9 this would be the 50^{th} image). This procedure is also repeated in the backward direction to label the images before the first LED occurrence, except the images are labeled in descending order. Figure 3.9 shows the labeling of approximately every sixth image. The end result of this process is a vector, shown in Figure 3.10, describing the number of the reference image set that corresponds to each image, for a given cycle. Since this process only defines the position vector for a particular cycle, it must be repeated for each cycle of the experiment.

3.2.3 Image Subtraction

After the position vector has been determined, the first ice image in the cycle is compared to the corresponding reference image. The comparison process involves the subtraction of the reference image from the ice image. Since each image is actually a matrix, this is only the subtraction of two matrices. It is assumed that any pixel in the ice image that is brighter than its corresponding pixel in the reference image must represent ice. This has been confirmed manually by comparing the results of the subtraction with the original two images.

Image subtraction is a common procedure in digital image processing used for two purposes, motion detection and background removal (Baxes, 1984; Jähne, 1993). For the digital image processing system described in this thesis, the subtraction process serves both purposes. It removes the uneven

background lighting and small scratches on the Plexiglas as well as detects changes between an image without ice and ones with ice.

The subtraction process is not perfect, as a result of the optical properties of frazil ice. It does not result in a precise solid shape representing a frazil particle. Rather, it produces frazil particles represented by blotchy shapes filled with holes surrounded by small random spots. However, it is effective in removing the scratches and the bright spot in the top left corner of ever image. Figures 3.11 (a), (b), and (c) show the reference image, the ice image, and the results of the subtraction process, respectively. An inspection of Figure 3.11 (c) shows how the subtraction process can actually "reveal" particles of ice masked in the bright zone.

The subtracted image/matrix is composed of zeros and both negative and positive numbers, with particles of ice maintaining higher positive values. If a pixel in the ice image was darker than its corresponding pixel in the reference image, then the resulting subtraction of the two pixels would yield a negative number. It has already been assumed that ice shows up as brighter pixels on the ice image, therefore a darker pixel in the ice image is assumed to be noise. As a result, negative entries in the subtracted image/matrix are changed to zero.

Low values in the subtracted matrix are also attributed to noise. Figure 3.12 shows a histogram of all the pixel values in fifty subtracted images created from an ice image, captured before any ice formed, and a reference image. Theoretically, every pixel in the subtracted image should be zero if there is no ice in the ice image, but under real conditions this does not always occur. The histogram shows that the subtracted image contains pixel values ranging from -4 to 3. Since no ice was present in these images, all these values must be attributed to noise. Therefore, any pixel value in the subtracted image with a value of three or less will be changed to zero. All other pixel values are considered ice particles and are changed to a one. This creates a binary image with ice particles represented by a one and the background represented with a zero. A binary image is required by many of the image processing functions and is easier to handle due to its low memory usage.

3.2.4 Image Dilation and Erosion

The binary image created from the subtraction process still includes some noise. The ice particles are blotchy, full of holes and there are random spots of noise scattered throughout the image. These

anomalies are rectified using three fundamental morphological operations: cleaning, erosion and dilation. Cleaning removes all pixels that have no neighbors, erosion removes pixels from an objects boundary, while dilation adds to its boundary. The number of pixels added or removed during dilation and erosion depends on the size and shape of the neighborhood or structuring element. The structuring element is a two-dimensional matrix composted of 0's and 1's. All entries in the structuring element with a value of 1 represent the neighborhood. The center pixel of the structuring element identifies the pixel of interest or the pixel being processed and is often referred to as the origin. Figure 3.13 illustrates some examples of structuring elements.

All three of these morphological operations start with an input image. The input image is the binary image created from the subtraction process. Each operation applies a set of rules using a structuring element to produce an output image. For dilation, the rule states that if **any** pixel in the input image's neighborhood is a 1, the corresponding pixel or the origin in the output image will also be a one. For erosion, the rule states that if **all** the pixels in the input image's neighborhood are 1's, the corresponding pixel in the output image will also be a one, else the pixel will be a zero. Figure 3.14 and Figure 3.15 show an example of the input and output images for the dilation and erosion operations, respectively. The structuring element used in this example and the actual processing system is a 3 by 3 matrix.

The processing of the binary image starts by cleaning the image. All pixels that are surrounded by 0's are removed from the image. As the name suggests this process cleans up the image by removing the stand-alone pixels that are not associated with any ice particles. Image processing continues by morphologically closing the image. This closing procedure is actually a dilation operation followed by an erosion operation, both using the same structuring element. The purpose of the closing operation is to fill in any gaps inside a frazil particle or connect any pixels immediately surrounding the particle. The closing procedure is immediately followed by an opening procedure which is an erosion operation followed by a dilation. The purpose of this procedure is to remove any small objects, such as the small noise elements, while still preserving the shape and size of the larger objects.

The closing function immediately followed by the opening function is essentially one dilation, followed by two erosions, and then finished with another dilation. These operations reduce the amount of noise and create coherent particles of frazil ice that are easily counted. Figure 3.16 a, b, c, d and e show the subtracted image, the binary image, the "cleaned" image, the image after applying

the morphological closing procedure, and the image after applying the opening procedure. Figure 3.17 shows a closer view of the same data as shown Figure 3.16.

3.2.5Particle Counting

The enhanced image, after the cleaning, opening and closing procedures have been conducted, is ready for the particle counting stage. MATLAB has a function in the image processing toolbox called *bwlabel* that labels connected components in a binary image (MATLAB, 2001). The enhanced binary image is entered as the input and the output is an integer matrix having the same dimensions as the original image. The background of the input image, which had a value of 0, retains the same number in the output matrix, while the individual particles are labeled with increasing integers. For example, the pixels that make up one complete, connected particle in the input image are all labeled with a 1 in the new output matrix, while the pixels from the next particle are all labeled with a 2, and so on. The highest integer in the output matrix is the total number of particles discretized by the function.

The next step is to measure and record the size and location of each individual particle. This information is recorded to a separate file for each image. For example, the size and location of a frazil particle on the n^{th} image taken during the m^{th} cycle can be recalled. This makes it possible to access the statistics about any image at any time. This is important because the analysis of the particle data is completed after all the images have been scrutinized.

The particle counting procedure is quite simple. All the entries or pixels in the output matrix with a specific integer are counted. For example, the total number of pixels with a value of 1 is counted, giving the size or area of that particle in pixels. This process is repeated for all of the integer values in the matrix. The location of the particles relative to the water surface is also a necessary piece of information. Assuming the particles are discoid in shape, the centroid is easily determined by averaging their extremities. The vertical centroid can be calculated using

$$\bar{y} = floor\left\{\frac{y_{max} - y_{min}}{2} + y_{min}\right\},$$

where $\bar{y}$ is the average pixel location in the vertical direction for the given particle, y_{max} is the maximum pixel location in the vertical direction for the given particle, y_{min} is the minimum pixel location in the vertical direction for the given particle.

3.2.6 Vertical Distribution of Ice

The change in the vertical distribution of ice is recorded by analyzing the enhanced binary images. The number of pixels in each row that represent ice is added together into one column vector. This vector represents the vertical distribution of ice for one image. Adding all the vectors produced from each image for a particular cycle creates a snapshot of the vertical distribution for a given time. Figure 3.18 illustrates the procedure used to calculate the vertical distribution of ice. In this figure, the enhanced binary image contains four separate particles marked with ones surrounded by a background of zeros. The ones in each row are added together and saved in the column vector.

3.2.7 Pixel Calibration and Conversion

The size and vertical location of each particle are recorded in units of pixels. It might seem odd that the area [L^2] and depth [L] of the particle are reported in the same units. To understand this incongruity, it is necessary to understand how CCD cameras operate. A CCD, Charge Coupled Device, is a small solid-state silicon device that is very sensitive to light. The CCD in the camera used to capture images on the flume has a nominal classification of 1/3", but is actually 4.88 mm x 3.66 mm. The CCD is composed of 325 546 small pixels each 7.4 μm x 7.4 μm. As light falls on each pixel, a charge pulse is produced that is measured by the CCD electronics and converted into an intensity value. The light intensity values are collected from all the pixels and organized to form a digital image.

Since each pixel on every image and on the CCD is square, the term pixel can be used to describe either an area or a length. For example, the size of a particle measured in pixels can be converted to an area by multiplying the frazil ice particle size in pixels by the area of one pixel. Likewise, the length of an object measured in pixels can be converted to a more meaningful number by multiplying it by the length of one pixel.

The size of a pixel on the CCD is very different from the size of the pixel on a digital image created by the CCD. The size of a pixel on a CCD will never change, but the size of a pixel on a digital image will change depending on the focal length of the lens on the camera. For example, if the camera is focused in on a small object, say a grain of rice, each pixel on the image may represent

0.02 mm, but if the camera is focused on a car, each pixel may represent 2 mm. Therefore it is necessary to measure the size each pixel represents in an image before trying to convert the size of an object in the image to mm or mm^2. This is easily accomplished by taking a picture of a ruler placed in the flume. The size of the image pixels can be determined by measuring the number of pixels in a 10 cm length on the ruler. Figure 3.19 illustrates this procedure. This calibration process only needs to be performed once, unless the camera's focal length or physical position are altered.

3.2.8 Summary of Image Acquisition Methodology

Pre-Experiment

- Capture 400 Images
- Create Reference Image Set based on LED signature

Experimental Data Collection

- Collect Ice Images and save to the computer

Post-Experiment

- Analyze LED signature on Ice Images to determine the position vector
- Subtract Ice Image from corresponding Reference Image
- Create Binary Image by changing all negative and low values to zero
- Enhance Binary Image using morphological procedures
- Count and size each particle
- Calculate vertical distribution

3.3 Data Analysis

The end result of the image processing system, after analyzing a complete experiment, is two data files. The first file contains the vertical distribution of ice particles for each cycle while the second file contains information about the individual frazil particles. The second file is created in such a way that the size and location of every particle can be recalled from any image. This storage method allows for flexibility in the examination of the results. The following section examines some methods and graphs that can be used to describe the results of the image processing.

3.3.1 Vertical Distribution

The vertical distribution information can be plotted three ways. First, a 3-D image can be created to display all the results on a single graph. Figure 3.20 shows an example of the 3-D image with the x-axis showing the elapsed time of the experiment beginning when the water reached a supercooled state, the y-axis shows the depth below the surface of the water, and the z-axis is labeled "Number of Pixels". The z-axis (vertical axis) represents the number of pixels at a specific depth that are interpreted as ice for one image. This type of image may be a nice way for an overview of each experiment, but it may be difficult to actually extract useful information from it. For a more detailed look at the data, cross-sections of this 3-D graph can be plotted. Figure 3.21 plots the vertical distribution of frazil ice for three specific depths, while Figure 3.22 plots this information for three specific times during the experiment. The actual depths and times used in these graphs is up to the user, but may be chosen to highlight specific events.

3.3.2 Particle Statistics

There are a number of different graphs that can be created to convey the results of the image analysis process. Figure 3.23 shows the average number of particles that were counted on each image for the duration of the experiment. This graph was generated by counting the total number of individual particles identified in one complete time cycle. This total number was then divided by the number of images captured for one time cycle, generating the average number of particles per image for a given time cycle. This process was repeated for each time cycle and the results were plotted with the time

scale on the x-axis and the average number of particles recognized on an image for each time cycle on the y-axis.

Figure 3.24 illustrates the evolution of the total area of frazil ice over the course of the experiment. The size of all the particles identified for a given time cycle are tallied to identify the total number of pixels that were recognized as ice. The total number of pixels was then divided by the total number of pixels in one cycle. The total number of pixels for one cycle is the number of pixels in one image, 307 200 (480x640), multiplied by the number of images in one cycle. The end result is the percent of the image that was occupied by ice. The results, as shown in Figure 3.24, are plotted with the time scale on the x-axis and the average particle area for each time cycle on the y-axis.

Another very important feature is the evolution of the particle size distribution. Figure 3.25 shows the particle size distribution for a given time cycle. The sizes of all the particles identified for a given time cycle are pooled together into one column vector. The particles are then split up into groups based on their size, generating a histogram as shown in Figure 3.26. Figure 3.26 shows a 3-D plot generated by graphing the histograms from each time cycle. The data in this figure was normalized by dividing the histogram for each time cycle by the number of images in the time cycle.

The information about the size distribution can also be plotted to isolate specific time cycles or specific depths. Figure 3.27 shows the size distribution for three separate time cycles while Figure 3.28 shows the data for three separate depths. The plots on these two graphs are essentially cross-sections of Figure 3.26.

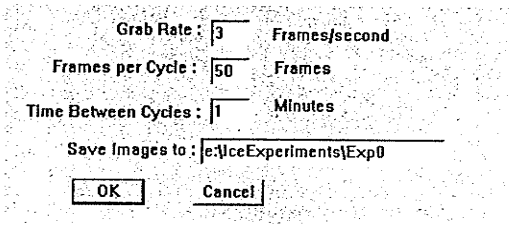

Figure 3.1. Input box for image collection program.

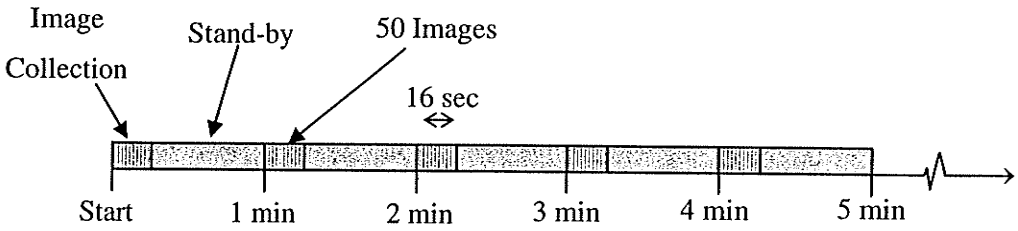

Figure 3.2. Typical image collection schedule.

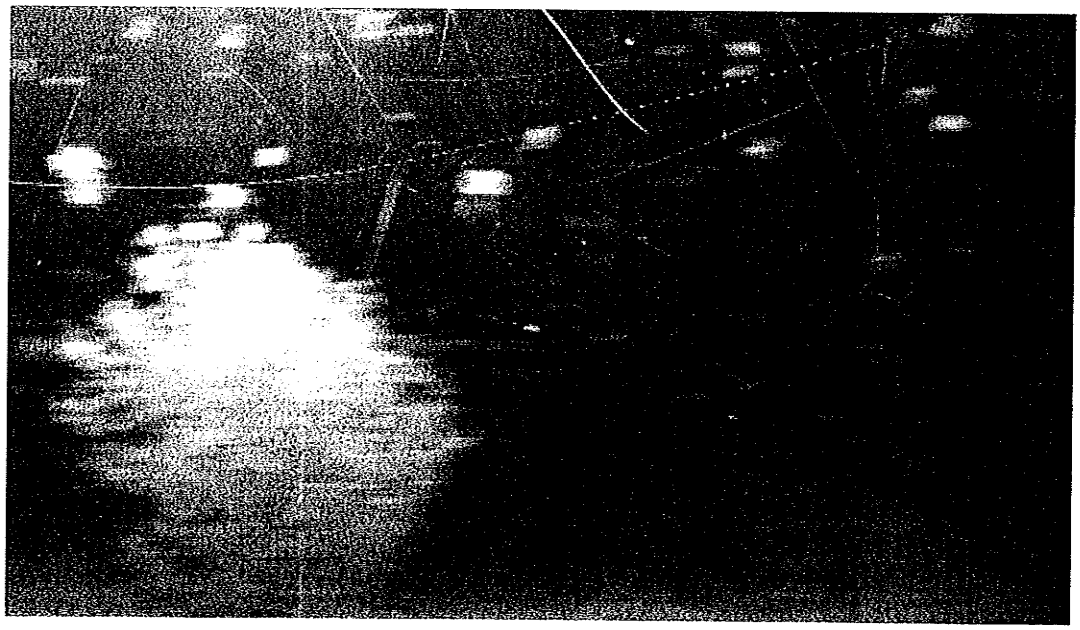

Figure 3.3. An image containing frazil ice particles

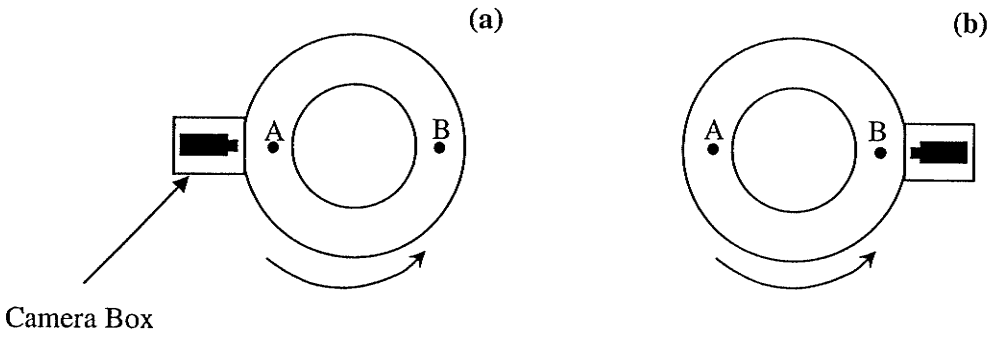

Figure 3.4. Camera location relative to the positions of **(a)** highest and **(b)** lowest image brightness.

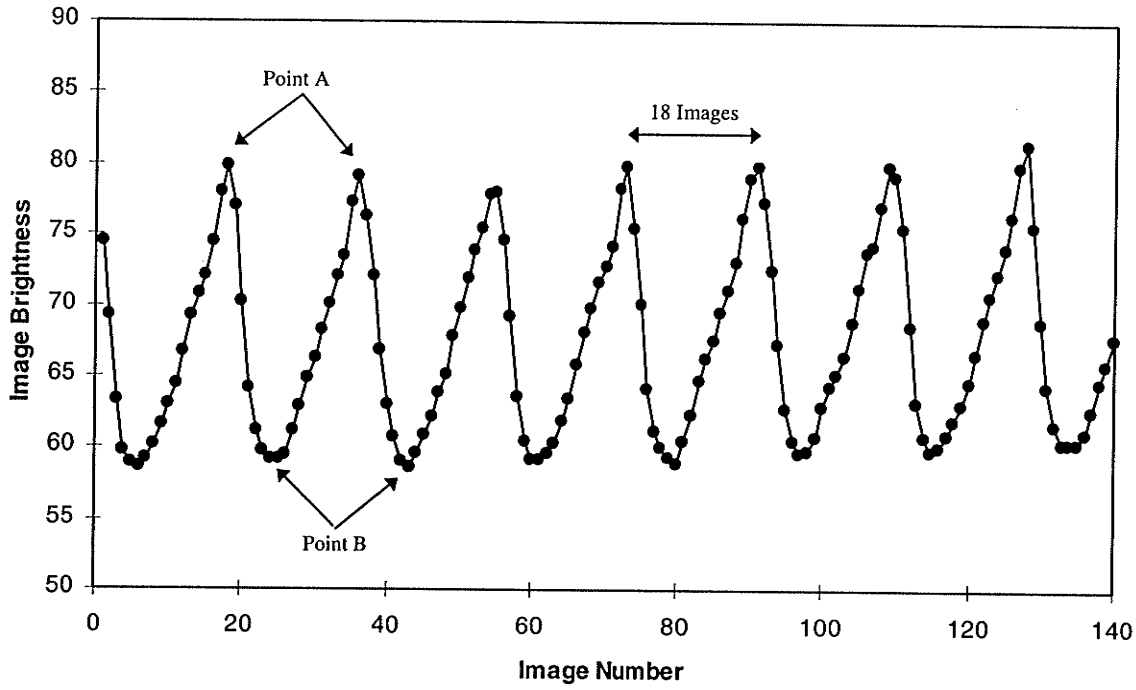

Figure 3.5. Average pixel brightness of the upper left quadrant of a series of images.

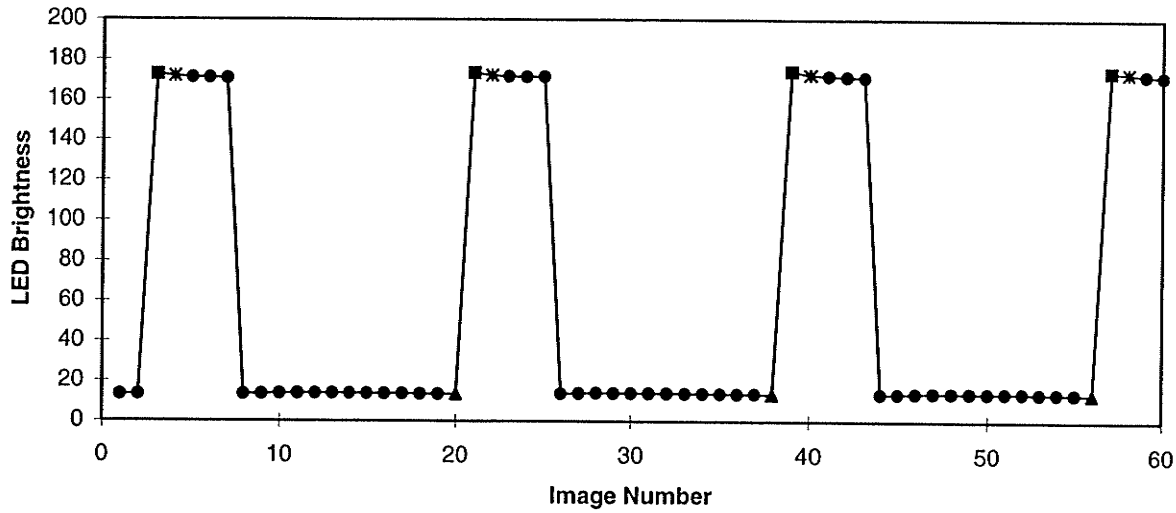

Figure 3.6. LED brightness for a portion of the 400 images used to create the Reference Image Set.

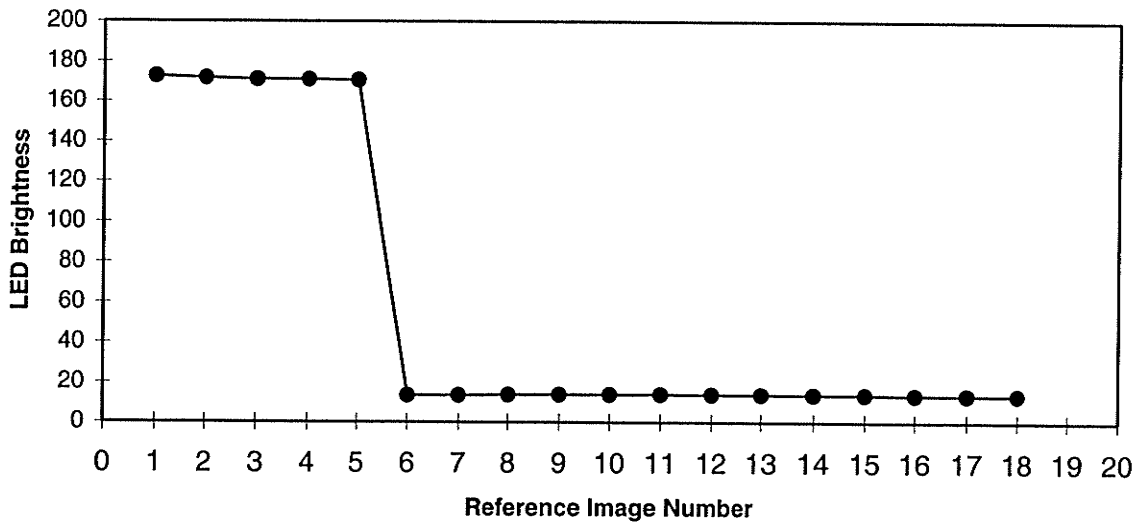

Figure 3.7. LED brightness for the completed Reference Image Set.

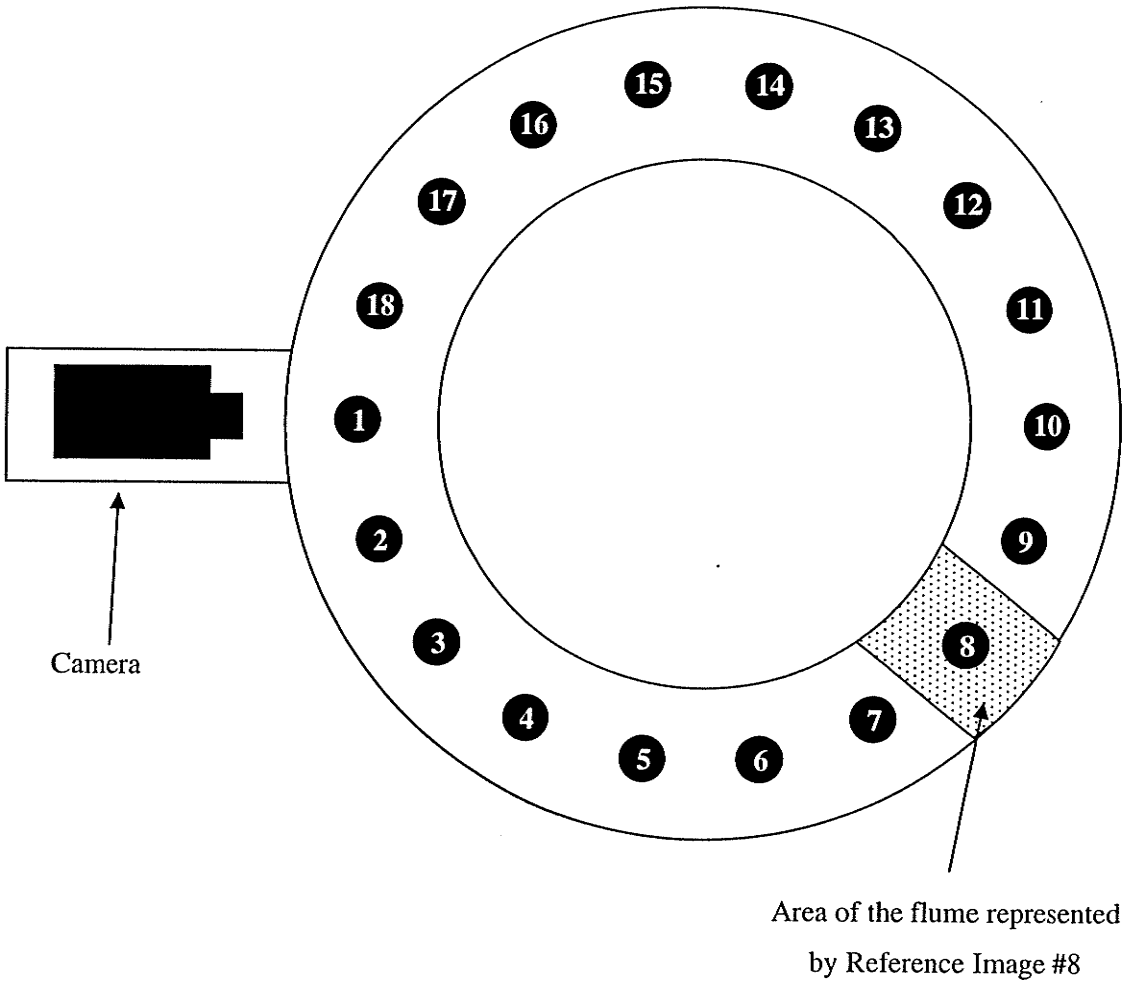

Figure 3.8. Outline of the flume illustrating the location where each reference image was captured.

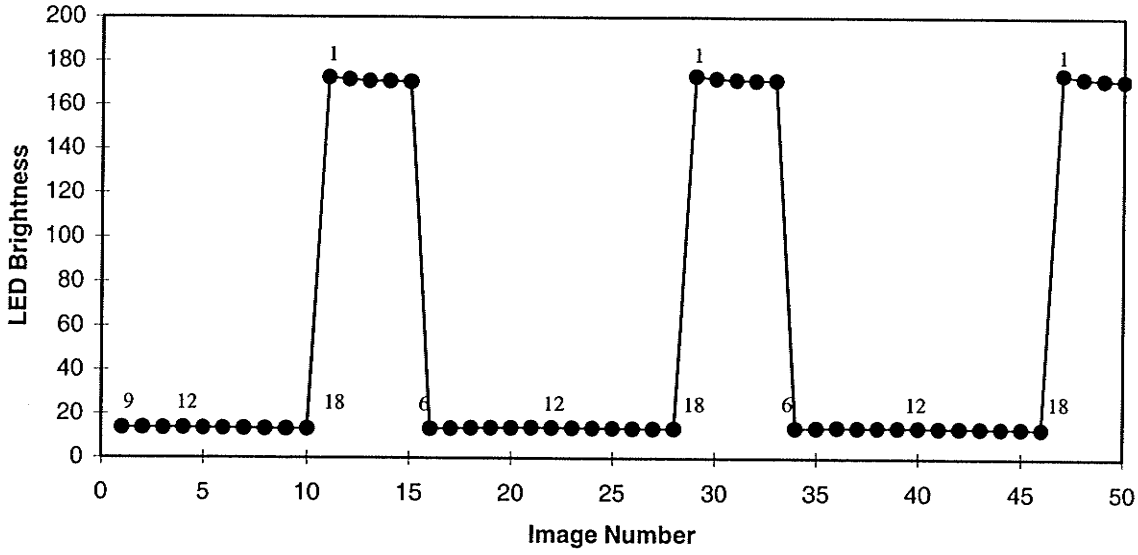

Figure 3.9. LED signature for one complete cycle of ice images with corresponding reference image labels.

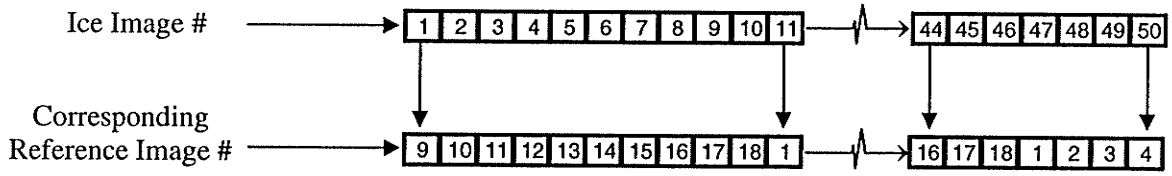

Figure 3.10. The vector representing the correct reference image to use in the comparison process for one complete cycle of 50 images.

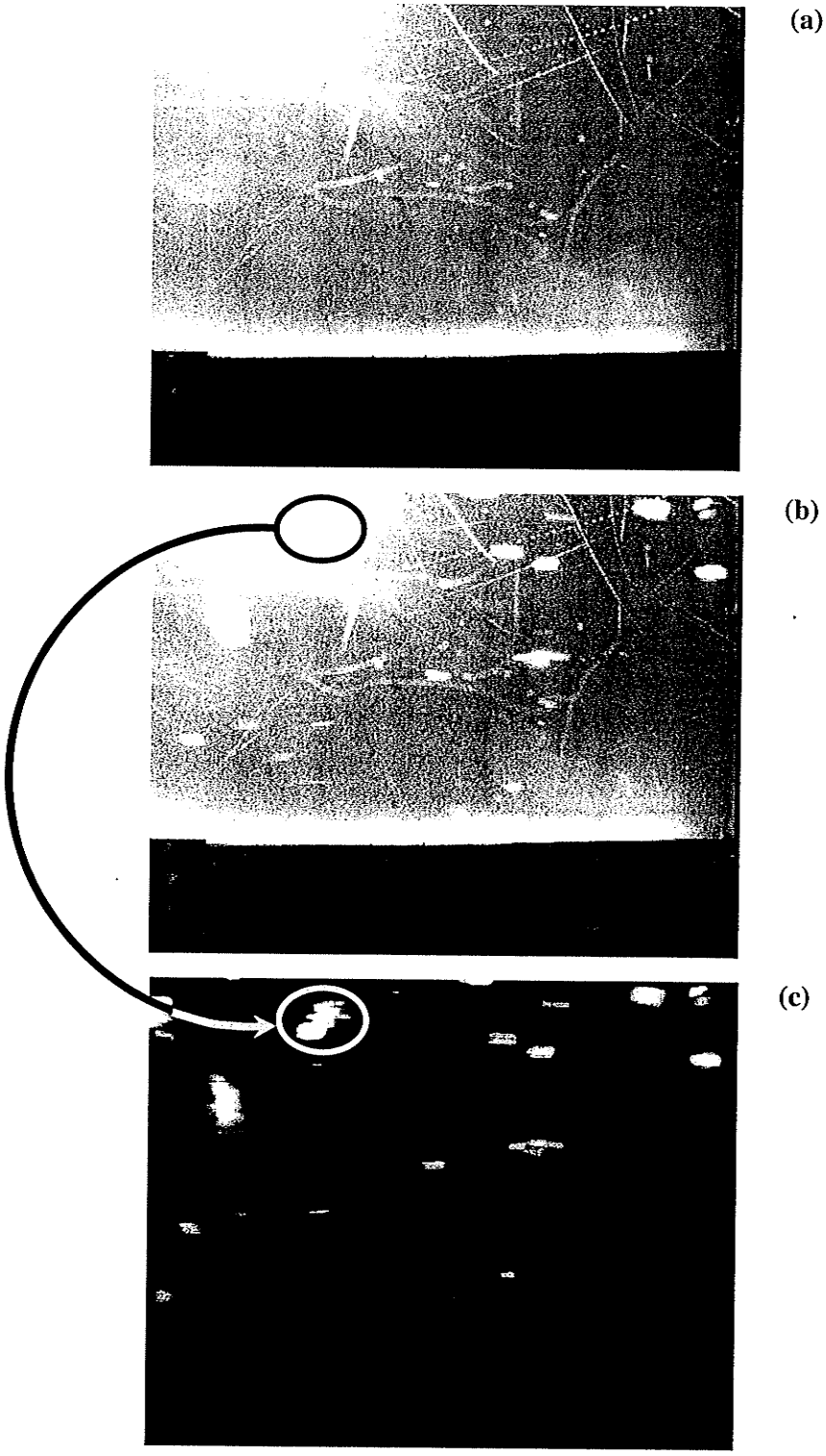

Figure 3.11. **(a)** The reference image, **(b)** the ice image, and **(c)** the results of the subtraction. Note the "revealed" particle of ice.

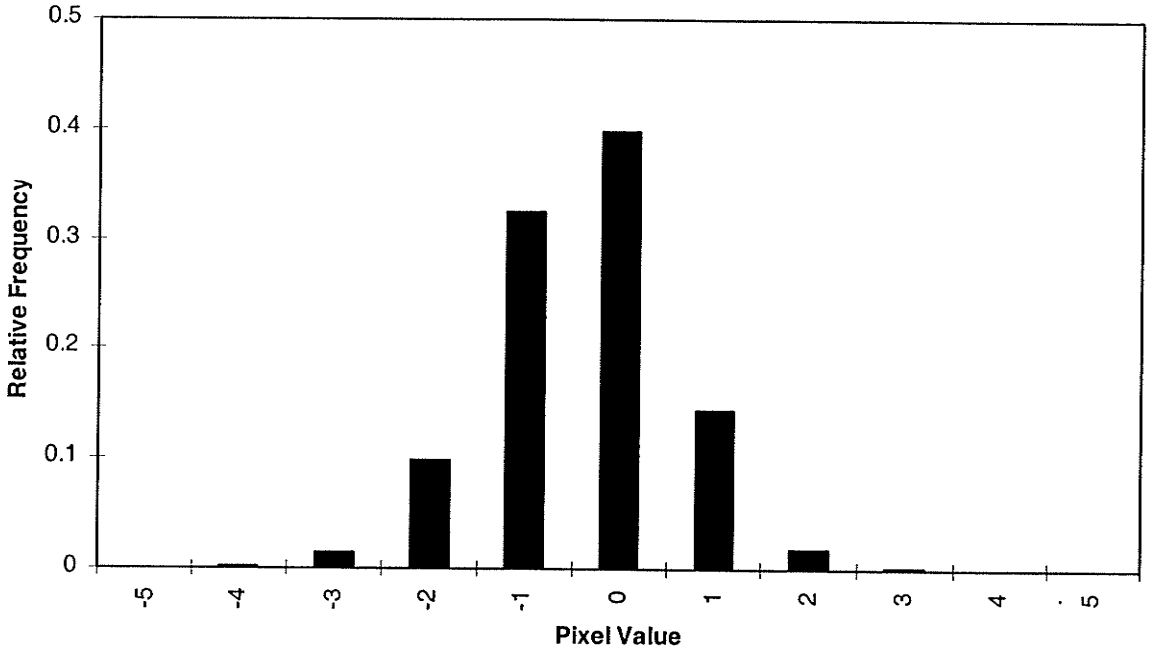

Figure 3.12. Histogram of the pixel values after reference image was subtracted from images that did not contain ice particles.

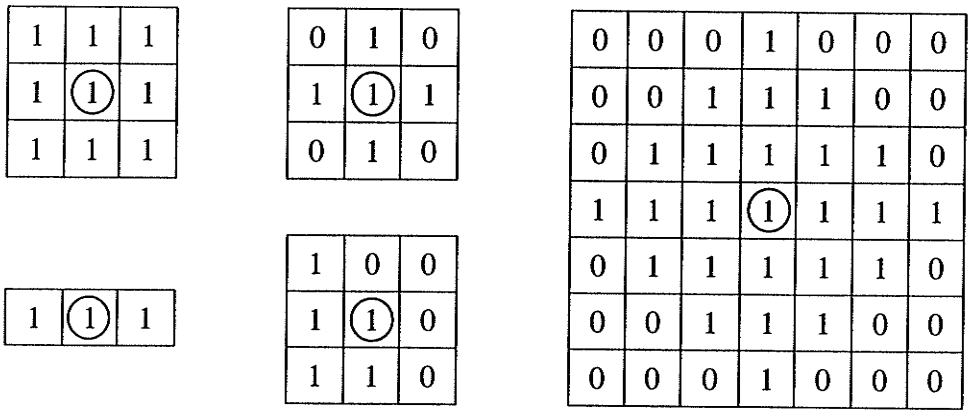

Figure 3.13. Examples of structuring elements, with the origin circled.

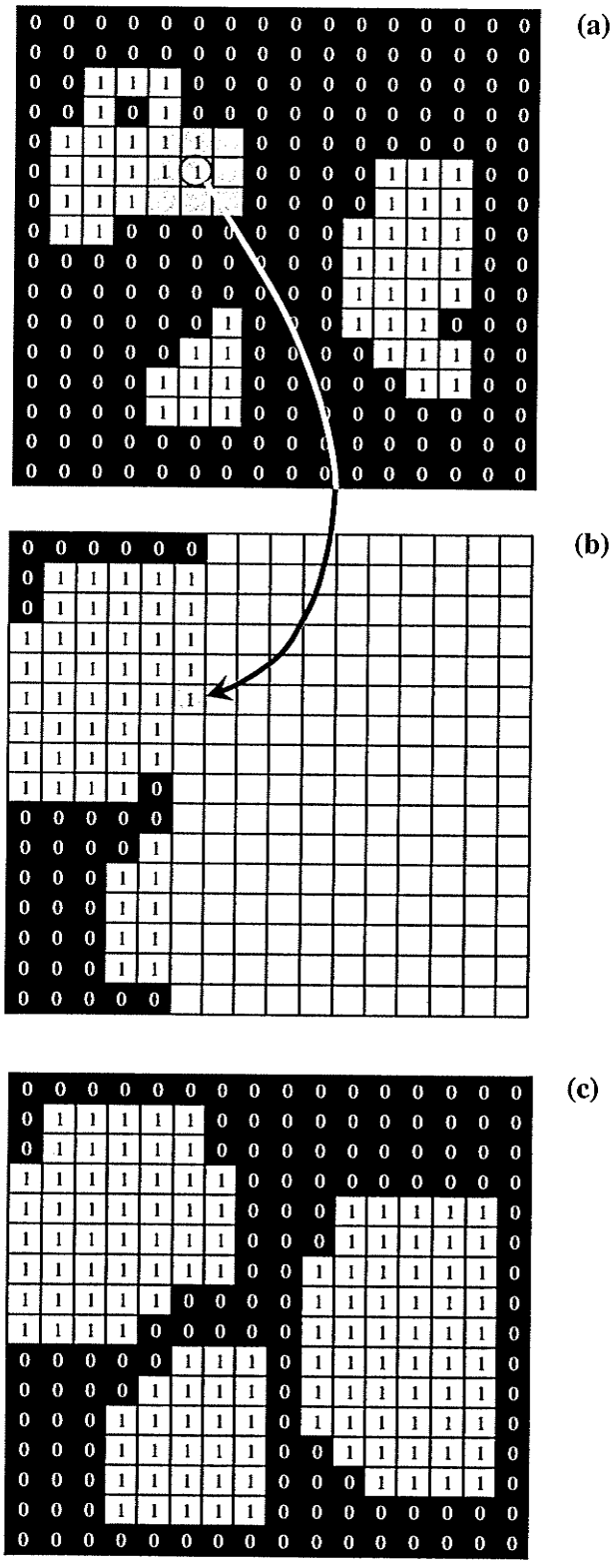

Figure 3.14. Dilation procedure using a 3x3 structuring element; **(a)** Original Binary Image with structuring element highlighted, **(b)** intermediate results, and **(c)** final output image.

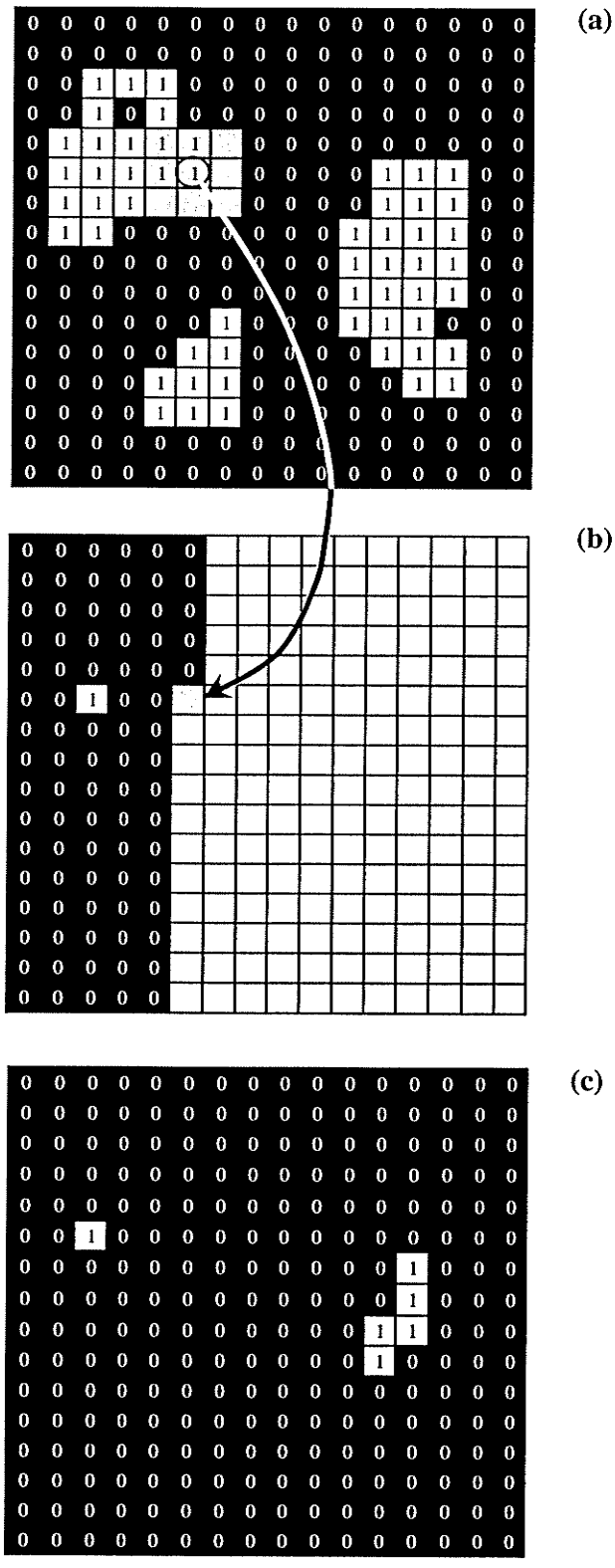

Figure 3.15. Erosion procedure using a 3x3 structuring element; **(a)** Original Binary Image with structuring element highlighted, **(b)** intermediate results, and **(c)** final output image.

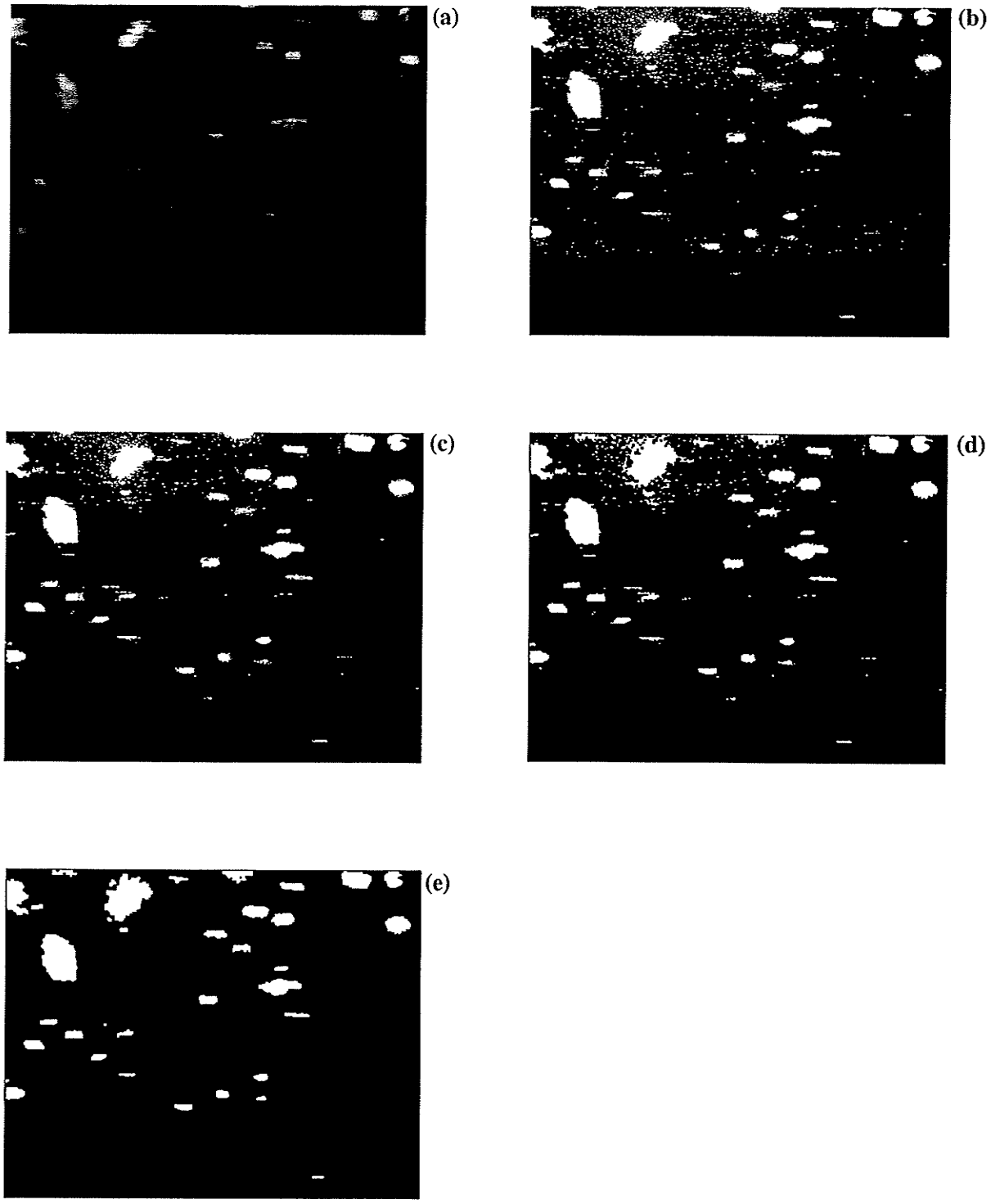

Figure 3.16. **(a)** Subtracted Image, **(b)** Original Binary Image, **(c)** Image after "Cleaning", **(d)** Image after closing, **(e)** Image after opening or the Enhanced Image.

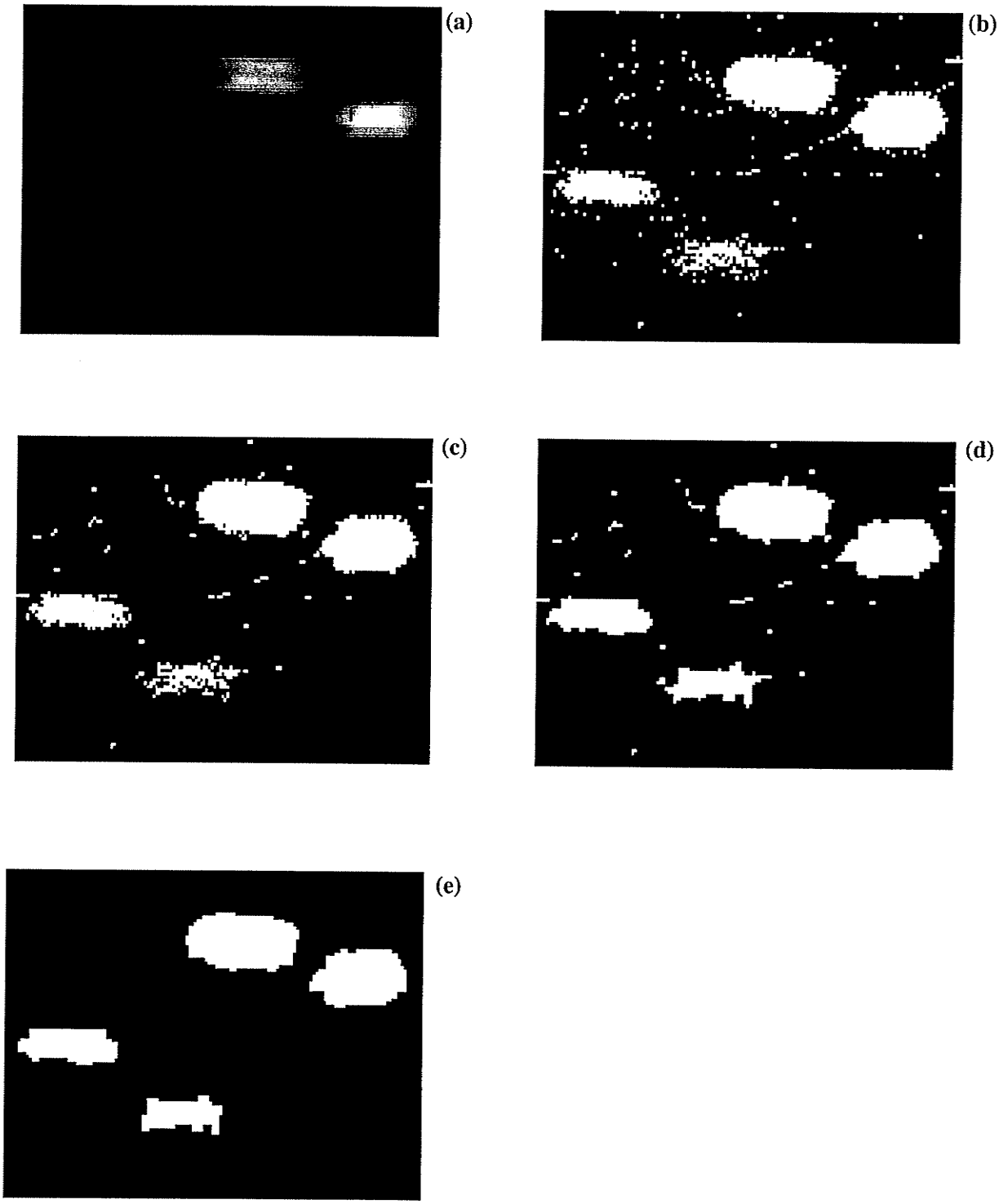

Figure 3.17. **(a)** Subtracted Image, **(b)** Original Binary Image, **(c)** Image after "Cleaning", **(d)** Image after closing, **(e)** Image after Opening or the Enhanced Image.

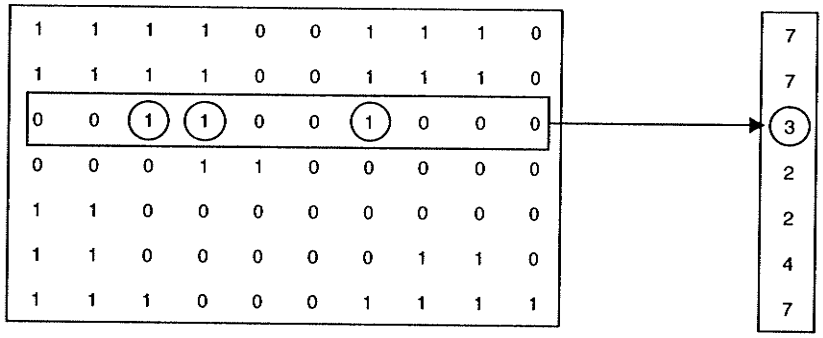

Figure 3.18. Example of method used to measure the vertical distribution of frazil ice.

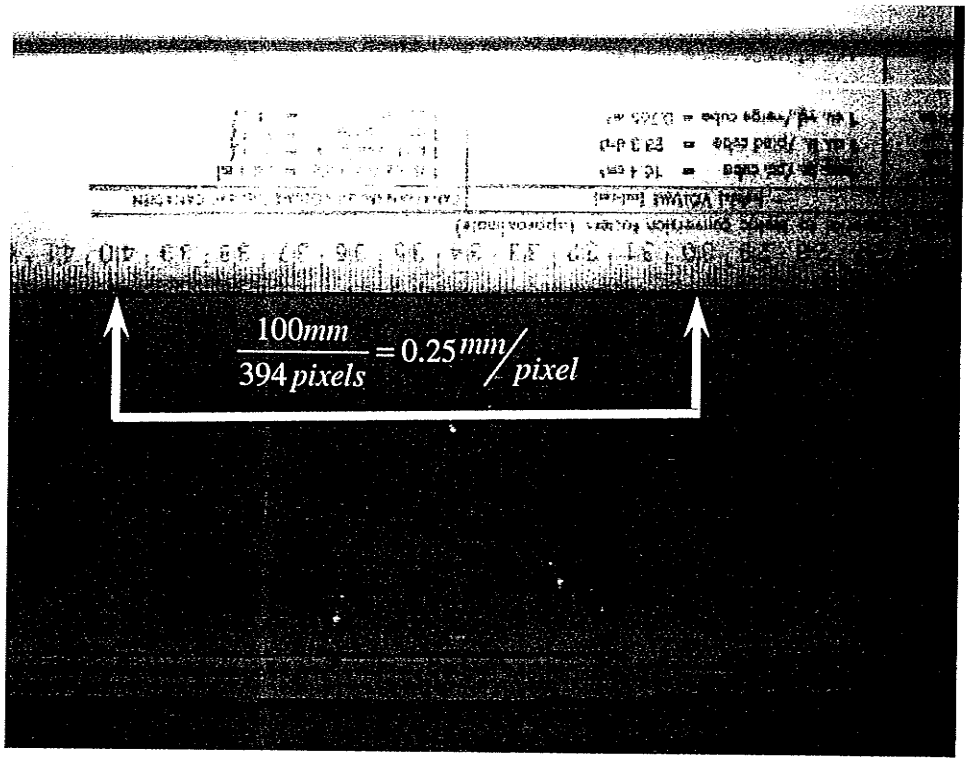

Figure 3.19. Calculation of pixel size.

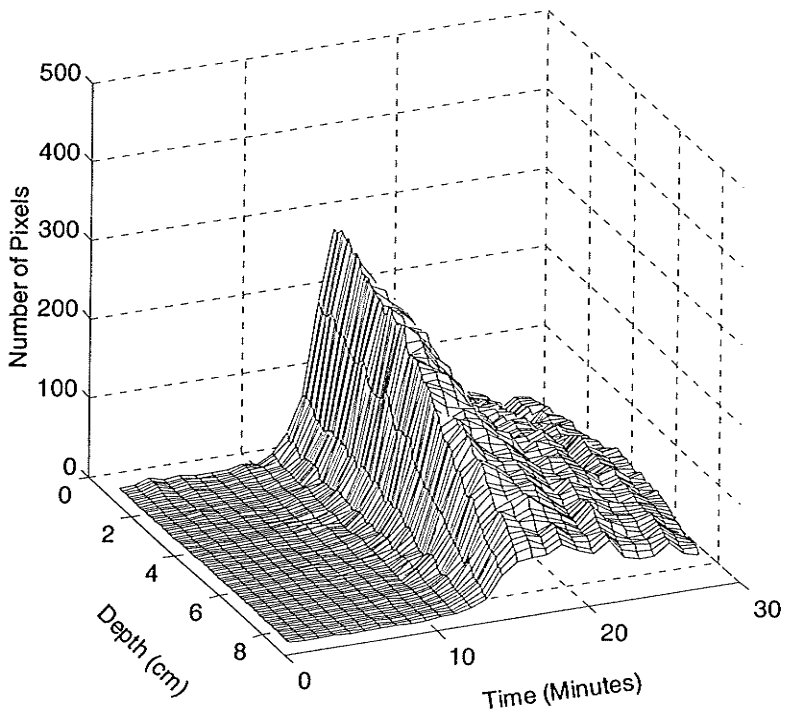

Figure 3.20. Time history of the vertical distribution of frazil ice using a 3-D plot.

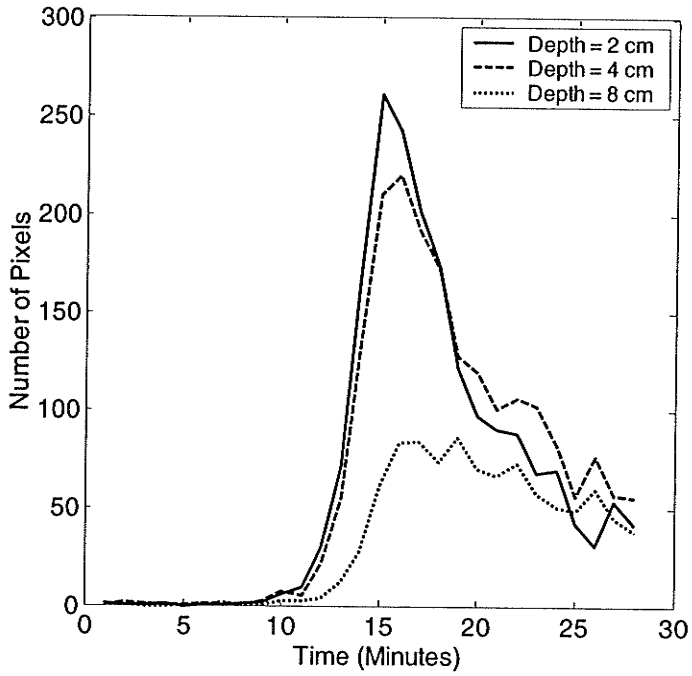

Figure 3.21. Time history of the vertical distribution of frazil ice for three specific depths.

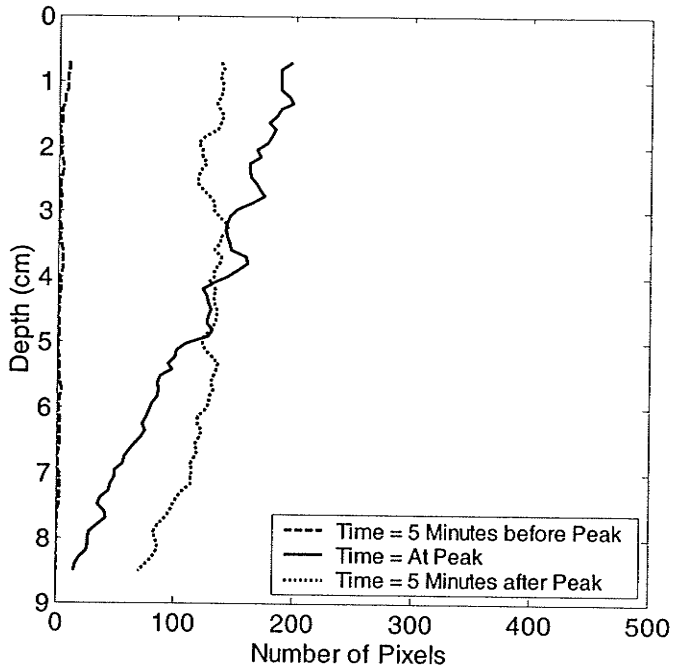

Figure 3.22. Vertical distribution of frazil ice for three specific times.

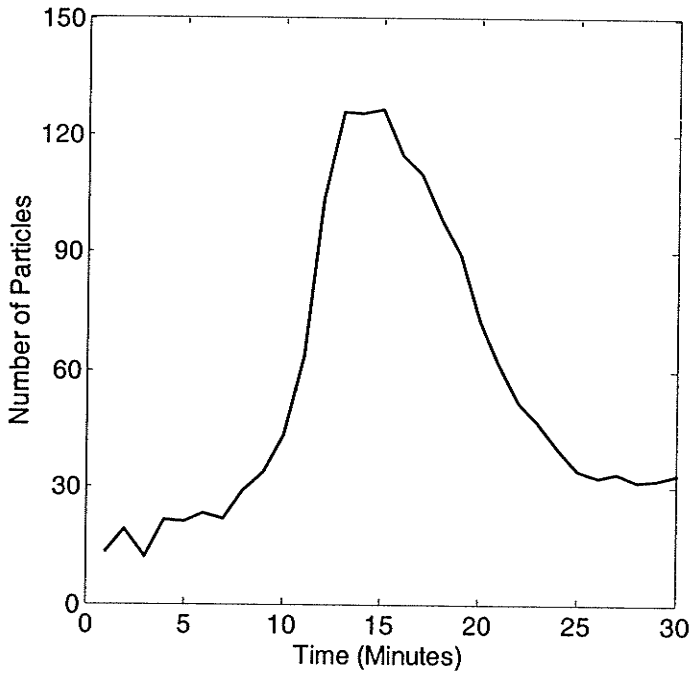

Figure 3.23. Average number of particles vs time.

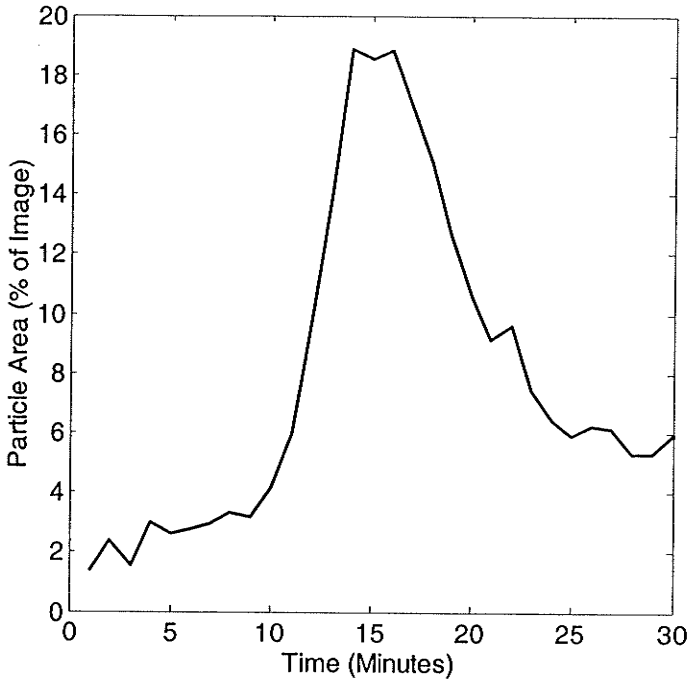

Figure 3.24. Average particle area vs time.

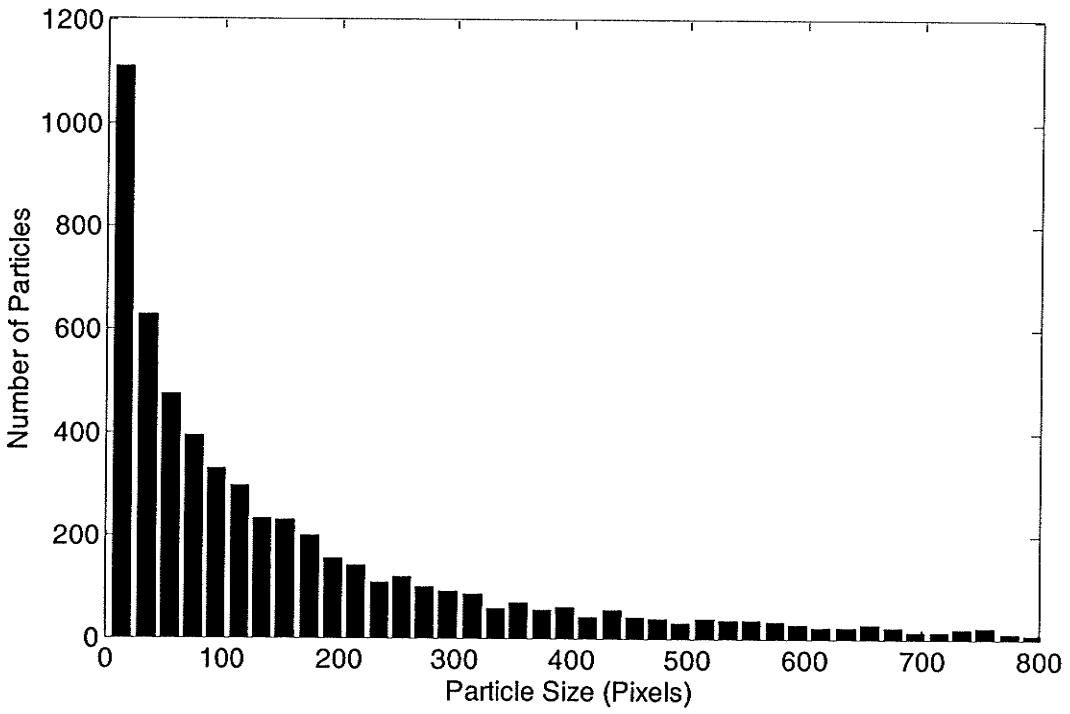

Figure 3.25. Particle size distribution for one time cycle.

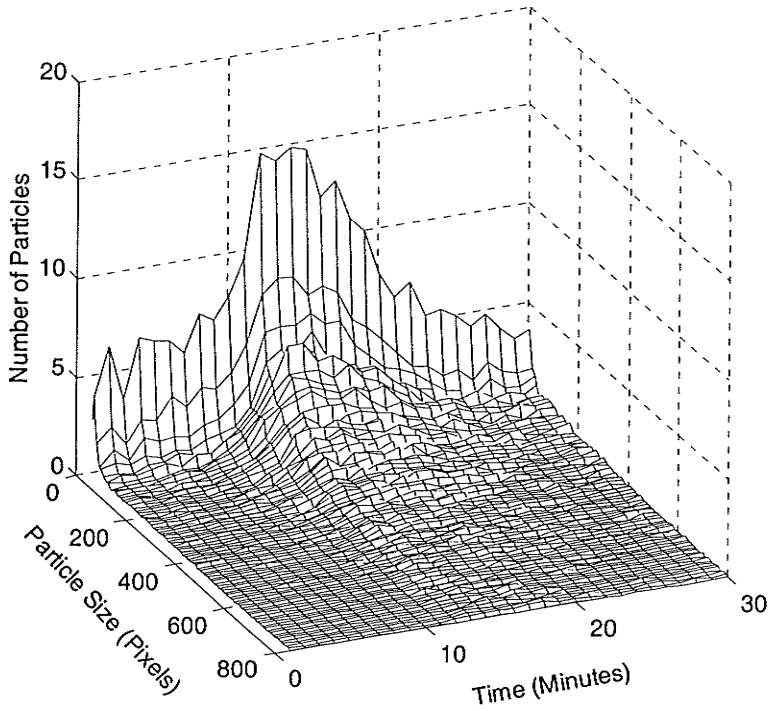

Figure 3.26. Particle size distribution for the entire experiment.

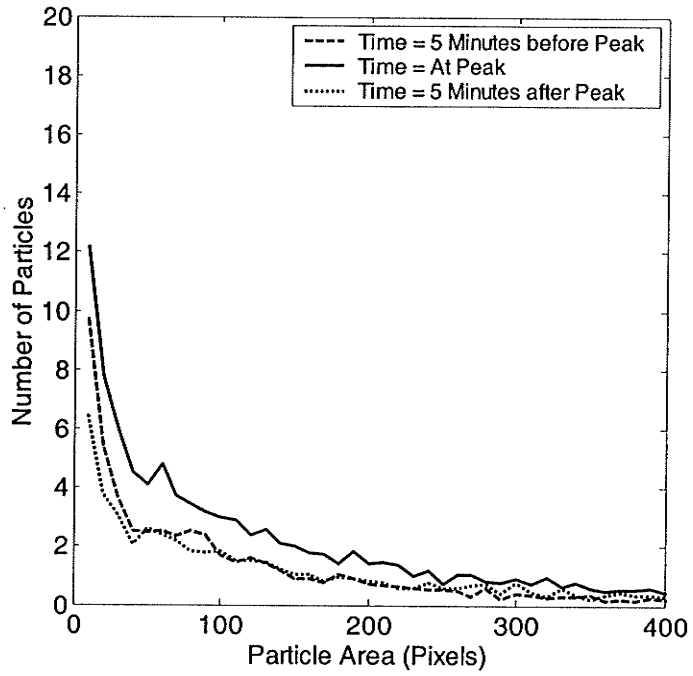

Figure 3.27. Particle size distribution for three specific times.

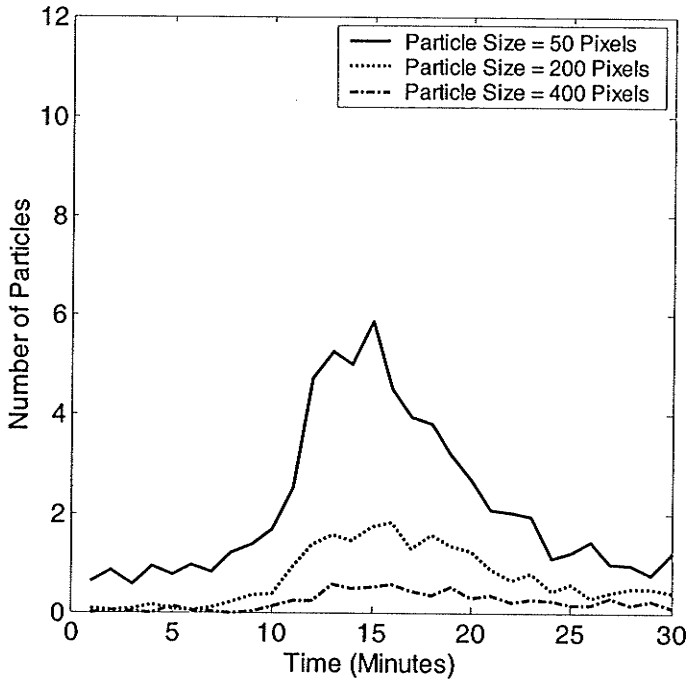

Figure 3.28. Particle history for three specific particle sizes.

CHAPTER 4

Process Validation and Experimental Testing

After the digital image processing system was developed, a series of ice experiments were conducted using the counter-rotating ice flume. The purpose of these experiments was to verify and validate the procedures used in the digital image processing system. The experiments were analyzed and frazil ice data was extracted and examined. As a result of this validation procedure, it was possible to make a qualitative description of the effects of water velocity and air temperature on the evolution of frazil ice particles. The emphasis of this thesis was the development of the digital image processing system, therefore the results of the experiments will not be rigorously examined to extract a conclusion about frazil ice processes, rather the results will be displayed, accompanied by a brief description.

A total of 12 experiments were collected using the counter-rotating ice flume at the University of Manitoba's Hydraulic Research and Testing Facility. Each experiment was conducted using either an air temperature of -15°C or -10°C and an effective water velocity of 70, 50, or 35 cm/s. At each air temperature, 6 experiments were collected, two experiments at each water velocity. This yielded 6 unique combinations of variables. Table 4.1 shows the variables used in each experimental run. Each experiment used the same image collection characteristics. The grab rate was 3 frames per second, the cycle length was one minute and 50 images were collected each cycle.

Table 4.1. Experiment Run Summary

Run	Air Temp °C	Water Velocity cm/s
1a	-15	70
1b	-15	70
2a	-15	50
2b	-15	50
3a	-15	35
3b	-15	35
4a	-10	70
4b	-10	70
5a	-10	50
5b	-10	50
6a	-10	35
6b	-10	35

4.1 Post Processing

Some experiments encountered a growth of ice on the Plexiglas walls. The ice initiated at the air/water/Plexiglas interface and progressed downward, even though the cavities surrounding the flume walls were heated. The extent of the downward growth of border ice varied for each experiment, ranging from zero ice growth to almost 3 cm. This caused a bright patch of ice to appear on the top of each image, which slowly evolved downward as the experiment progressed and was interpreted by the particle recognition process as a large ice particle floating on the surface. Figure 4.1 shows an ice image illustrating the surface ice growth phenomenon. Note the bright ice and the dimmer ice at the top of the image. The brighter ice is located on the back of the flume wall while the dull ice is attached to the front of the flume wall. In order to disregard the migration of ice on the flume walls from the image analysis, a portion of every image was not used. Obviously if ice growing on the flume walls can be seen in the first 50 lines of an image, then those lines should not be used in the image analysis.

The water temperature data collected using the RTD and data acquisition equipment required post processing. The meter used to convert the signal from the RTD into a digital signal was mounted on the side of the flume. The meter was enclosed in an aluminum case but was not insulated from the cold air temperatures produced by the cold room. The difference in air temperature for each

experiment caused the meter to deviate from its calibration curve. In order to compensate for this deviation, the water temperature data was analyzed after the experiment was completed and the temperature was adjusted by assuming that at the end of the experiment the water temperature reached a value of 0.0°C. The temperature data also contained some jitter, which required a smoothing average. The water temperature was smooth by averaging a 5 second window. Since the data was collected at 2 Hz, this was the average of 10 data points.

4.2 Experiment Repeatability

An important aspect of any experimental program is the repeatability of the results for the same given conditions. Since two experiments were collected at each of the six unique sets of variables, the repeatability can be determined by comparing the results of the two similar experiments ie., Run 1a and Run 1b. Two variables used to determine the repeatability of these experiments were the number of frazil ice particles and the total area of an image occupied by the detected ice particles.

As mentioned previously, there was a problem with ice growth on the walls of the flume that would be interpreted by the image analysis as a large particle of ice floating on the surface. If this ice were included in the particle recognition process, the results would be skewed in two ways. First, there would always be a very large particle counted in every image. This would increase the area of the image occupied by ice. Secondly, the ice growing on the walls will mask or hide actual particles floating on the surface. This will reduced the total number of particles recognized.

In order to make a fair comparison between experiments, any part of the image affected by the growth of ice on the wall should be ignored. In fact if any portion of any image is to be excluded from the analysis, then that portion of the image should be excluded from every image from every experiment. If one experiment ignores the first 100 lines of each image, while another experiment includes all portions of the image the results will be misleading. If both experiments have identical particle characteristics, but the first experiment excludes the top 100 lines due to ice on the flume walls, the results of the analysis will conclude that the second experiment produced more frazil ice particles. In reality, they both produced the same number of particles, but the first experiment had to ignore them because they were masked by the ice growing on the walls. Therefore, if any portion of any image of any experiment is ignored, the same portion must be excluded in every image of every experiment. A

visual inspection of the images near the termination of each experiment concluded that the first 100 lines of every image should be excluded from the analysis in order to compare all 12 experiments. The value of 100 rows was chosen because this was the furthest the ice progressed down the wall in any experiment.

Figure 4.2 and Figure 4.3 show the number of frazil ice particles detected and the area of each image occupied by ice for each set of unique variables. The time scale starts when the water first becomes supercooled. From these two figures it is clear that the experiments are relatively similar. The shape of the curves, the maximum values and the location of the maximum values are all relatively similar for each experiment conducted with the same experimental variables. The actual difference and percent difference in the peak values for the number of particles and for the particle area for each set of experiments are shown in Table 4.2. The differences in peak values for Run 3 and Run 6 for the particle area are not shown because these curves did not actually peak, but continued to climb. This attribute will be discussed shortly.

Table 4.2. Difference in Peak Values

Run	Number of Particles		Particle Area	
	Actual Difference	% Difference	Actual Difference	% Difference
1	0.4	0.3	2.6	13.6
2	5.1	5.0	2.9	25.9
3	11.1	22.8	-	-
4	7.8	7.5	5.2	32.2
5	1.0	1.5	0.1	0.7
6	11.5	36.8	-	-

The differences in peak values may be a result of slight differences in cooling rate. As reported, the cooling rates of each experiment were slightly different. This could lead to the differences in the number of particles or area of ice produced. Another aspect that could lead to the small differences could have been the water quality. The water in each experiment was taken from the City of Winnipeg's potable water system via a tap in the lab. The source of Winnipeg's water is Shoal Lake, 150 Km south east of Winnipeg on the Manitoba-Ontario border. Very little is done to purify the water with the exception of chlorination, consequently, the water used in the experiments contains some particulate matter. The experiments collected for this research were conducted over a three

month period. As a result, the water would sit in the flume for days or weeks without being used. Also, the water in the flume was periodically changed. Each time the water was changed, the concentration of particulate matter also changed. As well, each time the water sat around for an extended period, it will have picked up particulate matter from the air. It could be this varying amount of particulate matter in the water that causes the slight variations in peak values.

Another cause of the differences could have been the border ice growing on the sides of the flume walls, which may have affected the evolution of the ice in two ways. Small particles may have broken off into the flow acting as a seed for other particles to form. This could cause frazil ice to form sooner and in different quantities.

Although there are minor differences between the runs collected with the same water velocity and same air temperature, the experiments seem quite repeatable. The remainder of this chapter compares the differences of various frazil ice characteristics caused by the changes in air temperature or changes in water velocity. Since the experiments appear to be repeatable, only one of the experiments for a specific water velocity and specific air temperature will be used in the comparative process. Table 4.3 shows the Run names used in the remaining portion of this chapter. These experiments were chosen because they exhibited the least amount of ice growth on the walls of the flume. This allows for less of the images to be ignored. Figures 4.2 and 4.3 were analyzed by ignoring the first 100 rows of every image because that was the worst case for all the experiments. By choosing the Runs with the least ice growth, only the first 25 rows need to be ignored. This allows for more information to be extracted from each image.

Table 4.3. Experiments used in Comparative Process

Run #	Run Used
1	1b
2	2a
3	3a
4	4a
5	5b
6	6a

4.3 Observations/Discussion

4.3.1 Temperature Characteristics

The temperature characteristics of each experiment can be summarized with three statistics: cooling rate, period of supercooling, and degree of supercooling. The cooling rate was calculated by determining the slope of the temperature plot prior to the supercooling point. The second parameter, period of supercooling, measures the time each experiment was in a state of supercooling or below 0°C. The third parameter, degree of supercooling, measures the minimum temperature reached during the experiment. Table 4.4 shows these three parameters for each experimental run and Table 4.5 shows the three parameters averaged for each set of variables.

Table 4.4. Experiment Temperature Characteristics

Run	Cooling Rate °C/hour	Period of Super Cooling Minutes	Degree of Super Cooling °C
1a	-0.53	19	-0.060
1b	-0.48	20.5	-0.062
2a	-0.58	17.5	-0.048
2b	-0.49	21	-0.046
3a	-0.44	21	-0.041
3b	-0.59	24	-0.053
4a	-0.41	24	-0.040
4b	-0.34	21.5	-0.047
5a	-0.29	22.5	-0.047
5b	-0.30	23.5	-0.049
6a	-0.24	37.5	-0.047
6b	-0.31	30	-0.047

Table 4.5. Summarized Experiment Temperature Characteristics

Run	Cooling Rate °C/hour	Period of Super Cooling Minutes	Degree of Super Cooling °C
1	-0.505	20	-0.061
2	-0.535	19	-0.047
3	-0.515	23	-0.047
4	-0.375	23	-0.043
5	-0.295	23	-0.048
6	-0.275	34	-0.047

Figure 4.4 shows the cooling rates plotted against the water velocity. It appears that the cooling rate is strongly affected by the air temperature. The data shows that cooler air temperatures yield higher cooling rates for each water velocity. This result is expected since a cooler air temperature provides a larger heat sink that drives the cooling of the water surface. This result is similar to the results of Hanley and Michel (1977) who also concluded that the cooling rate is strongly affected by the surrounding air temperature.

From the data shown in Figure 4.4 it is unclear as to the effect of the water velocity on the cooling rate. It appears as though there may not be an effect at all but more data is needed before a definitive conclusion can be prepared. Hanley and Michel (1977) concluded that the velocity has a very weak influence on the cooling rate.

Figure 4.5 shows the length of the supercooling period plotted versus velocity for each experiment. This figure indicates that for each three velocities, the length of supercooling was longer for the warmer temperatures. Since the experiments conducted at the warmer temperatures also produced smaller cooling rates, a relationship might exist between the cooling rate and the length of supercooling. By plotting these two variables together, as in Figure 4.6, and fitting a linear curve to the data, it becomes apparent that larger cooling rates produce smaller time periods of supercooled water. This observation is similar to observations made by Carstens (1966).

Figure 4.7 shows the minimum temperature or the degree of supercooling achieved for each experiment. From this figure it appears there is no relationship between the degree of supercooling and the water velocity or the air temperature, but if the degree of supercooling is plotted against the

cooling rate, as shown in Figure 4.8, a trend appears. The apparent trend is quite small, but it is consistent with observations made by Carstens (1966) who concluded that as the cooling rate increased, the maximum supercooling temperature also increased.

4.3.2 Number and Area of Particles

Two important features of frazil ice evolution are the change in number and change in volume or concentration of frazil ice particles over the length of the experiment. The change in the number of ice particles is easily measured by simple counting the number of particles on each image. The change in volume of ice is not as straightforward to measured. The image processing system can measure the area of ice particles observed simply by counting the number of pixels excited on each image. To convert the area of ice particles seen on a 2-D image into a volume of ice requires some assumptions about the shape of the frazil ice particles. Because the shape and density of the frazil particles change as it grows and differs depending on the flow and atmospheric conditions (Ashton, 1986; Daly, 1984), this task of converting an area seen on an image to a volume of ice becomes quite difficult. Due to the difficult nature of this assumption, no conclusive conjecture will be made. Therefore, instead of reporting the evolution of the volume of ice, the area of ice is presented.

Temperature Effects

In an effort to examine the effects of temperature on the number and total area of frazil ice particles, the experiments are separated according to the water velocity, thereby isolating the air temperature as the variable. Figures 4.9 **(a)**, **(b)** and **(c)** show the number of frazil ice particles generated for the three experiments conducted at 70 cm/s, 50 cm/s and 35 cm/s, respectively. The time scale starts at the point of initial supercooling. For each experiment, the shape of the basic curve is relatively consistent for each experiment, mainly, the number of frazil ice particles in the water column increased drastically, then decreased almost as drastically. Although this basic trend is apparent in all of the six conditions, there does appear to be a difference in some of the curve characteristics such as the peak number of particles and the time of this peak.

The peak number of frazil ice particles appears to be greater for the cooler temperatures. For each of the three velocities, the peak number of particles detected is approximately 30% greater when the air temperature was -15°C. The time of the peak also varies considerably. The peak in frazil ice

particles for the experiments conducted at -15°C occurred 3 to 5 minutes sooner than the experiments conducted at -10°C.

The effect of temperature on the area of frazil produced is also apparent in Figures 4.9 **(d)**, **(e)** and **(f)**. The cooler air temperature seems to produce more ice with the peak occurring sooner. The shape of the curves is also similar for a constant velocity.

The differences seen in Figure 4.9 are attributed to a change in air temperature from -10°C to -15°C. This does not imply that the same level of differences would be seen for any 5°C change in temperature. The differences would probably be different if the air temperature changed from -15°C to -20°C or from -5°C to -10°C. It is unknown if the changes in frazil production would be linear in response to a linear change in air temperature. Therefore, instead of making quantitative conclusions about the effects of temperature, only qualitative inferences will be made. From the data collected it appears that as the air temperature decreases, the peak number and area of particles increases. It also appears that the peak occurs a few minutes later.

Velocity effects

To isolate the changes in frazil production due to the changing velocity of the water, the experiments are separated into two groups. The first group consists of the three experiments conducted at an air temperature of -15°C while the second group contains the three experiments tested at -10°C. Figures 4.10 (a) and (b) show the number of frazil particles produced for each group with the time scale beginning at the point of supercooling. A large difference in the peak number of frazil particles is clearly apparent. As the velocity increases, so does the maximum number of frazil particles. This observation is consistent with conclusions made by Hammar and Shen (1994), Osterkamp (1978), Ettema (1984). As the velocity increases so does the turbulence. The increased turbulence increases the transfer of heat from the frazil particles to the surrounding water and also increases the rate of floc rupture (Ettema, 1984). This increase in the rate of floc rupture greatly increases the nuclei in the water from which new frazil particles can form (secondary nucleation). Figures 4.10 (a) and (b) also show that as the velocity increases, the peak in particles occurs sooner.

Figures 4.10 (c) and (d), which show the area of ice observed, also indicate that the velocity has a significant effect on the area of frazil produced. The larger velocities seem to produce more particle

area. The experiments conducted at 70 and 50 cm/s show a rapid rise in frazil area followed by a similar rapid decline in the area. This may seem conflicting that the frazil area decreases after it reaches a maximum value, but one must remember that this variable is not reporting the volume or mass of frazil ice, rather it is reporting the total projected area seen by the camera.

The total volume or mass of frazil ice will not decrease as the experiment progresses, but will increase until a layer of ice forms at the surface. Once this layer of ice forms, it acts like an insulator, preventing the water from cooling. This drastic reduction in energy loss prevents frazil ice from forming. Although the mass of ice cannot decrease, the total projected area of the frazil particles, as seen on the images, may decrease. There are two reasons to explain this occurrence, particle overlap and particle capture.

The images collected in these experiments are 2 dimensional pictures of the water column. The width of the flume is 20 cm, which means the camera is looking through 20 cm of water. An individual particle of ice observed on an image is actually the projected area of the frazil ice particle. If two particles of ice are suspended in the water, there is a chance that their projected image may overlap as seen by the camera. If this were the case, the particle recognition process would identify the two particles as one particle.

The probability of overlapping particles of ice depends on the number of ice particles, the size of the particles, and their distribution within the water column. The probability of overlapping particles increases as the number and size of the particles increase. Also, a poor distribution of particles will increase the chance of overlap.

Higher water velocities produce more frazil ice particles. Since the formation of particles happens rapidly, the size of the particles will generally be smaller and will therefore be more easily influenced by turbulence. This ease of influence, coupled with larger levels of turbulence, causes the particles to be distributed almost evenly throughout the water column. Conversely, at lower velocities the particles will be larger and not as easily influenced by turbulence. Since the levels of turbulence are reduced, the particles will generally be located near the surface, increasing the chance of overlap.

The second reason explaining the decrease in projected particle area is particle capture. After the initial formation of frazil ice particles, the crystals begin to agglomerate into flocs (Ashton, 1986). As the experiment continues, the flocs themselves start to stick together forming larger flocs. The

projected area of two identical particles will not equal the projected area of a larger particle formed from the first two particles. For example, if two small spherical particles stick together to form a larger spherical particle, the volume of the larger particle will be the sum of the two smaller particles but the projected area of the larger particle will be more than 20% smaller the sum of the projected areas of the two smaller particles.

At the lower velocity (35cm/s), the frazil area does not peak, rather it slowly continues to increase (Figure 4.10 (c) and (d)). This is contrary to the experiments collected at the higher velocities which experienced a large peak followed by a decline. One possible explanation is the lower velocity and lower levels of turbulence exert smaller forces on the flocs of frazil ice which reduce the chances of floc rupture. This leaves the flocs "fluffier", with large voids or interstices and generally float to the surface. This leads to a poor distribution of particles and increases the chances of particle overlap. Not only do the particles overlap, but they tend to flocculate together.

Velocity has a large impact on the number and area of frazil ice particles. During the peak in frazil ice production, the higher velocities produced more particles. This was also the case for the area of ice detected with the exception of the lower velocities. At lower velocities the frazil area did not peak, but climbed continuously. This feature was only apparent at the lowest velocity, but occurred for both temperatures.

Timing

Another interesting feature is the timing of the explosion of frazil ice particles. Figure 4.11 shows the number of particles plotted along with the temperature history. In every experiment, the explosion of frazil ice particles coincided with the rise in temperature. As the temperature of the water decreases, it passes through 0°C and continues to cool. A few minutes after the water has become supercooled, the rate of temperature decline begins to diminish. The time between the point of supercooling to the drop in cooling rate depends on many factors including the air temperature, water cooling rate and water velocity, but is typically around 10 to 15 minutes. This reduction in the cooling rate coincides with the initial appearance or nucleation of frazil ice. The cooling rate continues to drop until it reaches zero. At this point the water has reached it lowest temperature. The water temperature then rises while the number of frazil ice particles increases drastically. As the water temperature approaches 0°C, its rate of increase asymptotically decreases until the rate is zero at 0°C. At this

point the heat lost from the surface of the water to the cold air is in equilibrium with the heat gained from frazil ice formation.

4.3.3 Particle Depth Observations

An interesting feature in frazil ice research is how the vertical distribution of ice changes as frazil ice evolves. At the start of frazil formation, the particles are very small and float around in the water column under the influence of small turbulent eddies. As the particles increase in size and number, they begin to collide and stick together forming bigger particles called flocs. The turbulent influence on these larger flocs is reduced, allowing the flocs to float to the surface. There are two reasons that larger flocs are influenced less by turbulence. The first factor is related to the size. The larger a particle is, the larger the eddy has to be in order to move it. This phenomenon can be observed in a river. Small rocks and sand are easily suspended and transported in a turbulent river, while larger rocks with similar densities cannot be suspended. The second factor that affects the turbulent influence is related to the structure of the frazil ice flocs. A frazil floc is not a solid particle; rather it is quite porous (Ashton, 1986). Although the flocs have a high porosity, the structure of the floc is reasonably effective in restricting the movement of water between the interstices. Therefore, as the flocs grow over time, the static water in the pores freezes, increasing the buoyancy causing it to float to the surface.

Figure 4.12 shows the distribution of ice within the water column for the history of each experimental run. The x-axis is the elapsed time of the experiment beginning when the water reached a supercooled state, the y-axis is the depth below the surface of the water, and the z-axis is labeled "Number of Pixels". The z-axis (vertical axis) represents the number of pixels at a specific depth that are interpreted as ice for one image.

As explained in Chapter 3, the quantity of ice at a given depth was calculated by adding up all of the pixels in each row that represent ice. Since each row on an image contains 640 pixels, this is the maximum value that can be attained. The maximum value would be reached if ice covered the entire width of the image. From Figure 4.12, the maximum number of pixels observed for any row is about 450 for Run 3.

The 3D diagrams shown in Figure 4.12 were created for a quick visual inspection. For a more detailed look at the depth distribution, cross-sections of the 3D diagrams were created. Figure 4.13 shows the average number of pixels observed at three different depths. At each depth for the experiments conducted at 70 and 50 cm/s, the peak and subsequent decline in ice generally occurred at the same time. At the peaks, the concentration of ice was higher at the surface and declined as the depth increased. During this moment the frazil particles are still relatively small and are easily influenced by turbulence and buoyancy. As the experiment progresses, the ice particles start to agglomerate or stick together, eventually forming two or three large flocs that may cover the entire water column from the surface to the bed. These large flocs continue to grow in size as they gradually collect all the newly formed frazil particles. This phenomenon was visually confirmed as the experiments were in progress, but is also confirmed by the data collected. Figures 4.13 (a), (b), and (c) show that near the end of the experiment, all three depths reported nearly the same concentration of ice.

At the lower velocity, shown in Figures 4.13 (c) and (d), the vertical distribution of ice was quite different. The peak seen in the higher velocities was not apparent; rather the concentration seemed to increase throughout the experiment, but only at certain depths. As the depth increases, the concentration of ice decreases. At this low velocity, there is not sufficient turbulent energy to fully mix the frazil ice particles to the bottom of the water column. The large flocs observed near the completion of the 70 and 50 cm/s experiments are not present for the runs at 35 cm/s. This was also confirmed through visual observations

4.3.4 Particle Size Observations

Figure 4.14 shows the particle size distribution for each experimental run. The x-axis is the elapsed time of the experiment beginning when the water reached a supercooled state; the y-axis is the size of the particle measured in pixels, while the z-axis shows the number of particles identified within each size bin. The data shown in this figure is the average size distribution for one image produced by averaging 50 images.

For a more detailed look at the size distribution, three intervals were isolated and a histogram of the particle sizes was produced. Figure 4.15 shows the particle size histograms 5 minutes before the peak in particles, at the peak and five minutes after the peak. In each experiment for every time period, the

dominant particle size was the smallest particle. The smallest particle detectable by the image processing system is about 10 pixels, which works out to be approximately 0.6 to 0.8 mm diameter. Daly and Colbeck (1986) measured particle size distribution using a microscope that could detect particles as small as 0.03 mm diameter. They concluded that the distribution of frazil ice particles followed a log normal distribution. It is possible that the distribution of particles in Figure 4.15 follows a log normal distribution but due to the current limitations of the image processing system, the distribution of the smaller particles (< 10 pixels) is unknown. Therefore the distribution classification of the particle sizes cannot be made.

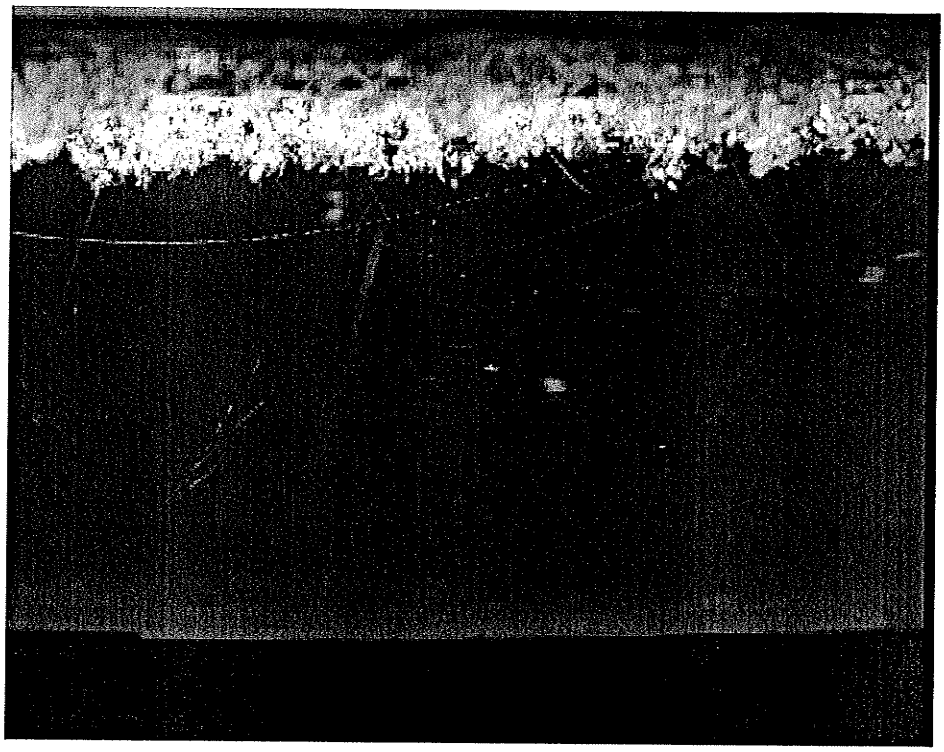

Figure 4.1. Ice attached to the wall near the surface.

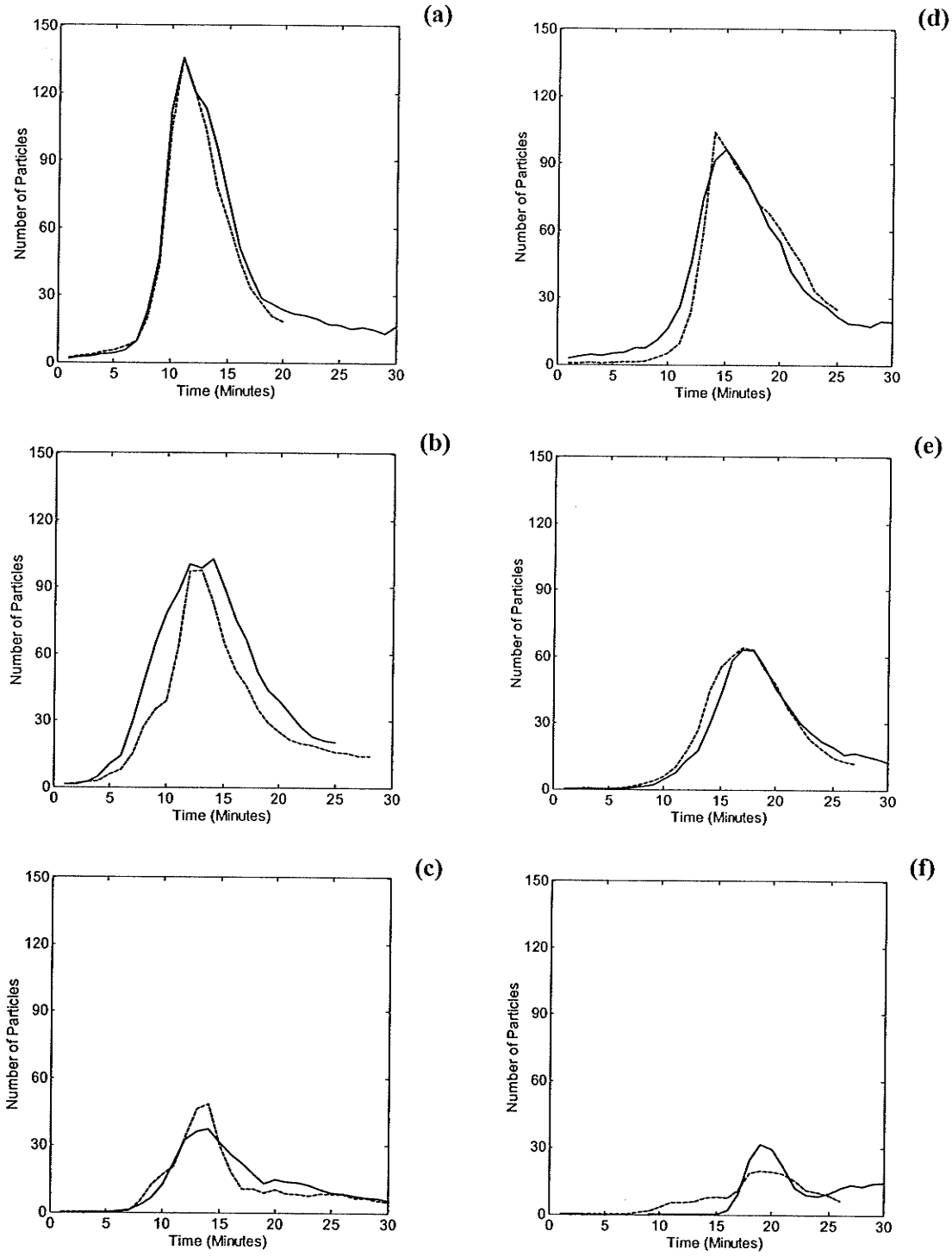

Figure 4.2. Time series of the number of particles detected for **(a)** Run 1, **(b)** Run 2, **(c)** Run 3, **(d)** Run 4, **(e)** Run 5 and **(f)** Run 6. The solid line (——) denotes Run A for the set while the dashed line (- - -) denotes Run B.

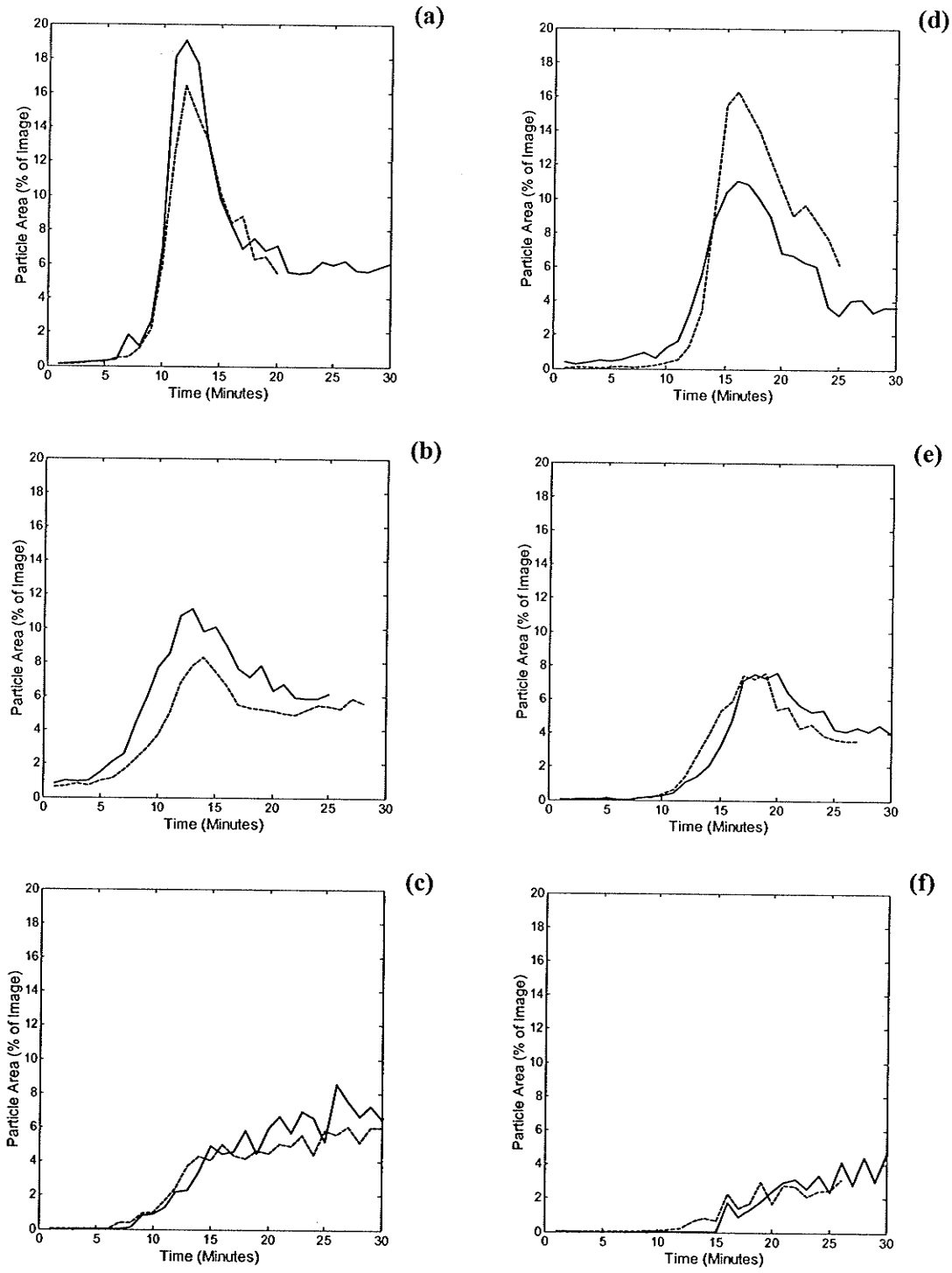

Figure 4.3. Time series of the particle area detected for **(a)** Run 1, **(b)** Run 2, **(c)** Run 3, **(d)** Run 4, **(e)** Run 5 and **(f)** Run 6. The solid line (——) denotes Run A for the set while the dashed line (- - -) denotes Run B.

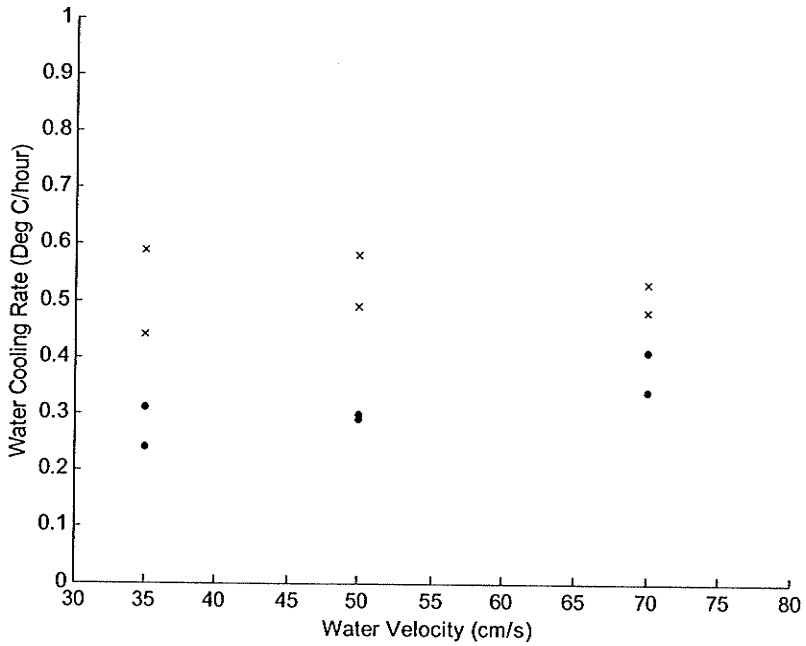

Figure 4.4. Water cooling rate vs. water velocity at air temperature = -10°C (•) and air temperature = -15°C (x).

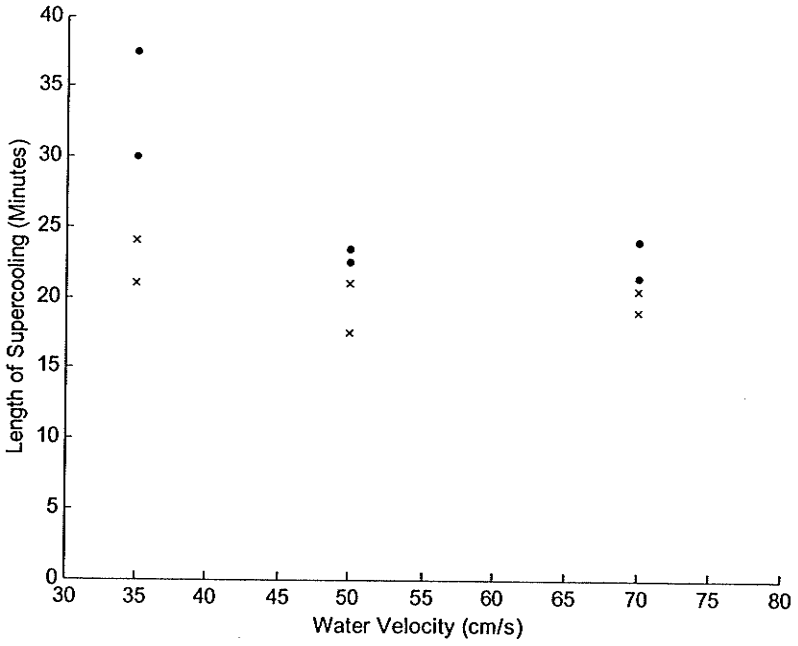

Figure 4.5. Length of supercooling vs. water velocity at air temperature = -10°C (•) and air temperature = -15°C (x).

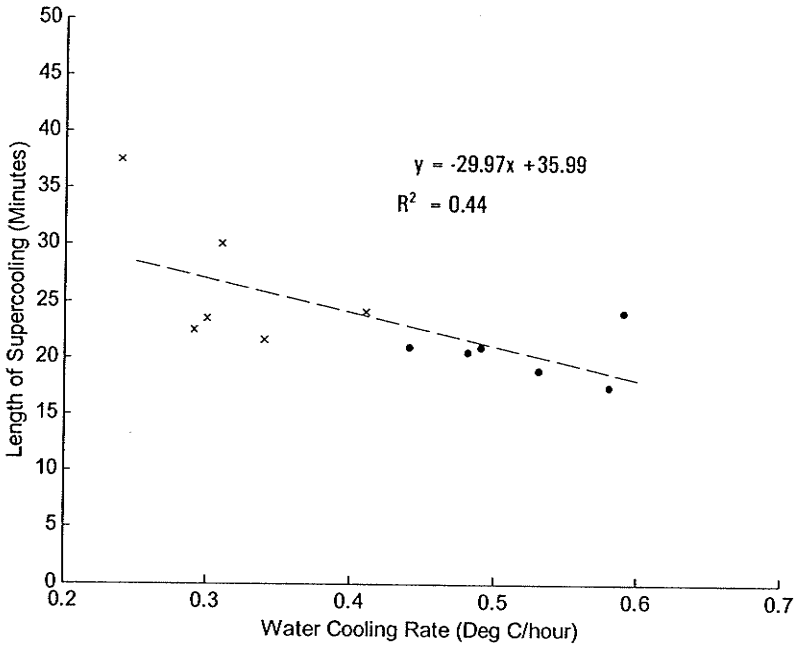

Figure 4.6. Length of supercooling vs. water cooling rate at air temperature = -10°C (•) and air temperature = -15°C (x).

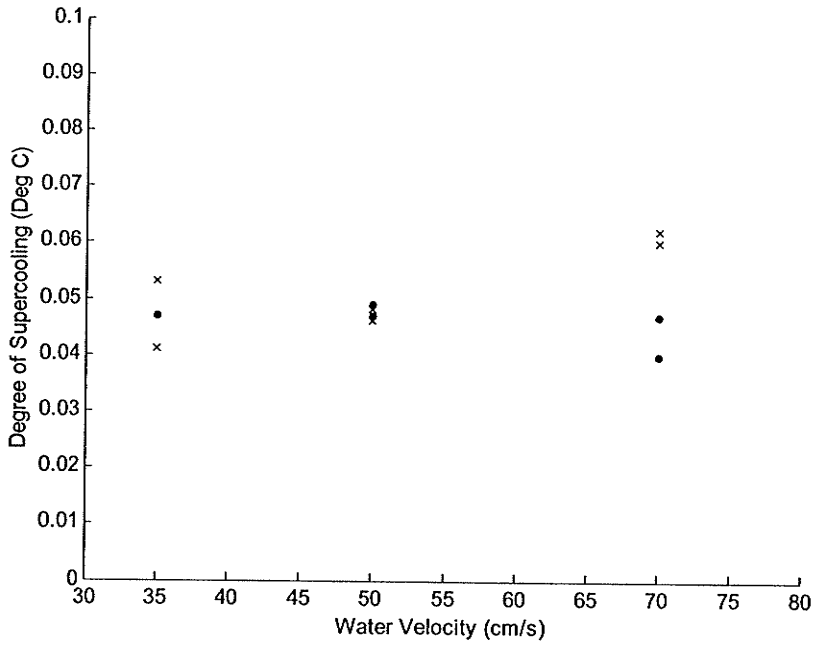

Figure 4.7. Degree of supercooling vs. water velocity at air temperature = -10°C (•) and air temperature = -15°C (x).

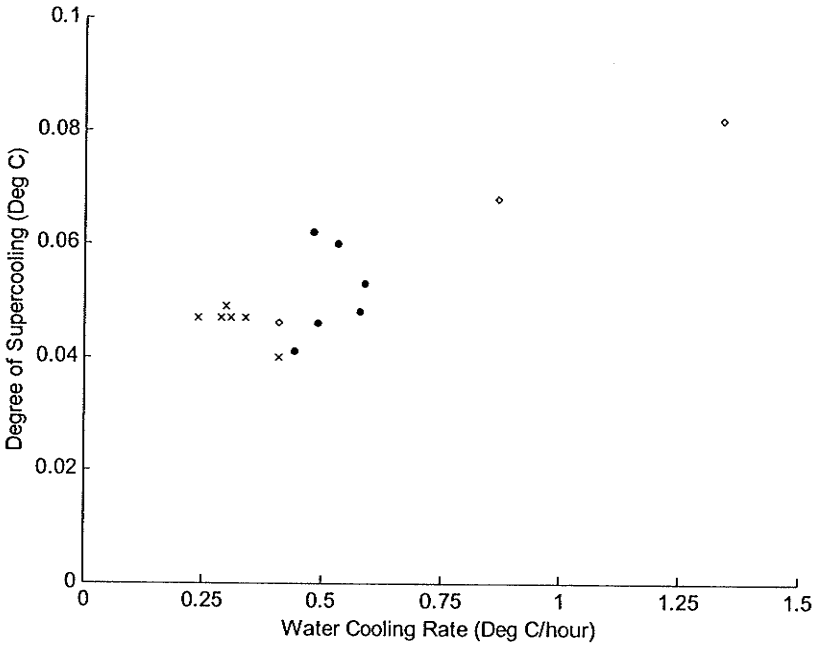

Figure 4.8. Degree of supercooling vs. water cooling rate at air temperature = -10°C (•), air temperature = -15°C (x) and Carstens' (1966) experimental data (◊).

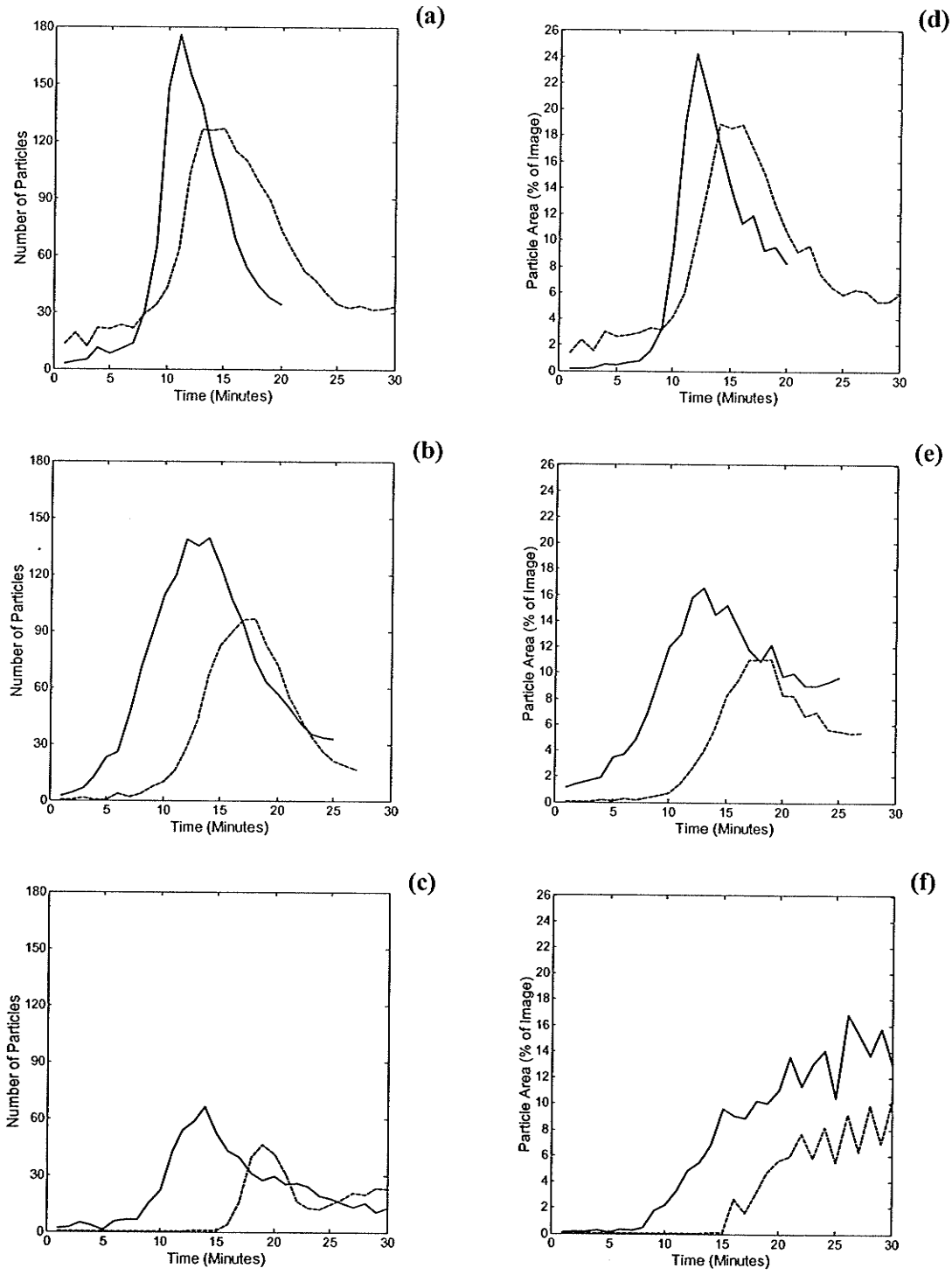

Figure 4.9. Time series of the number of particles at **(a)** velocity = 70 cm/s, **(b)** velocity = 50 cm/s, **(c)** velocity = 35 cm/s, and particle area at **(d)** velocity = 70 cm/s, **(e)** velocity = 50 cm/s, and **(f)** velocity = 35 cm/s. The solid line (——) denotes air temperature =-15°C while the dashed line (- - -) denotes air temperature of -10°C.

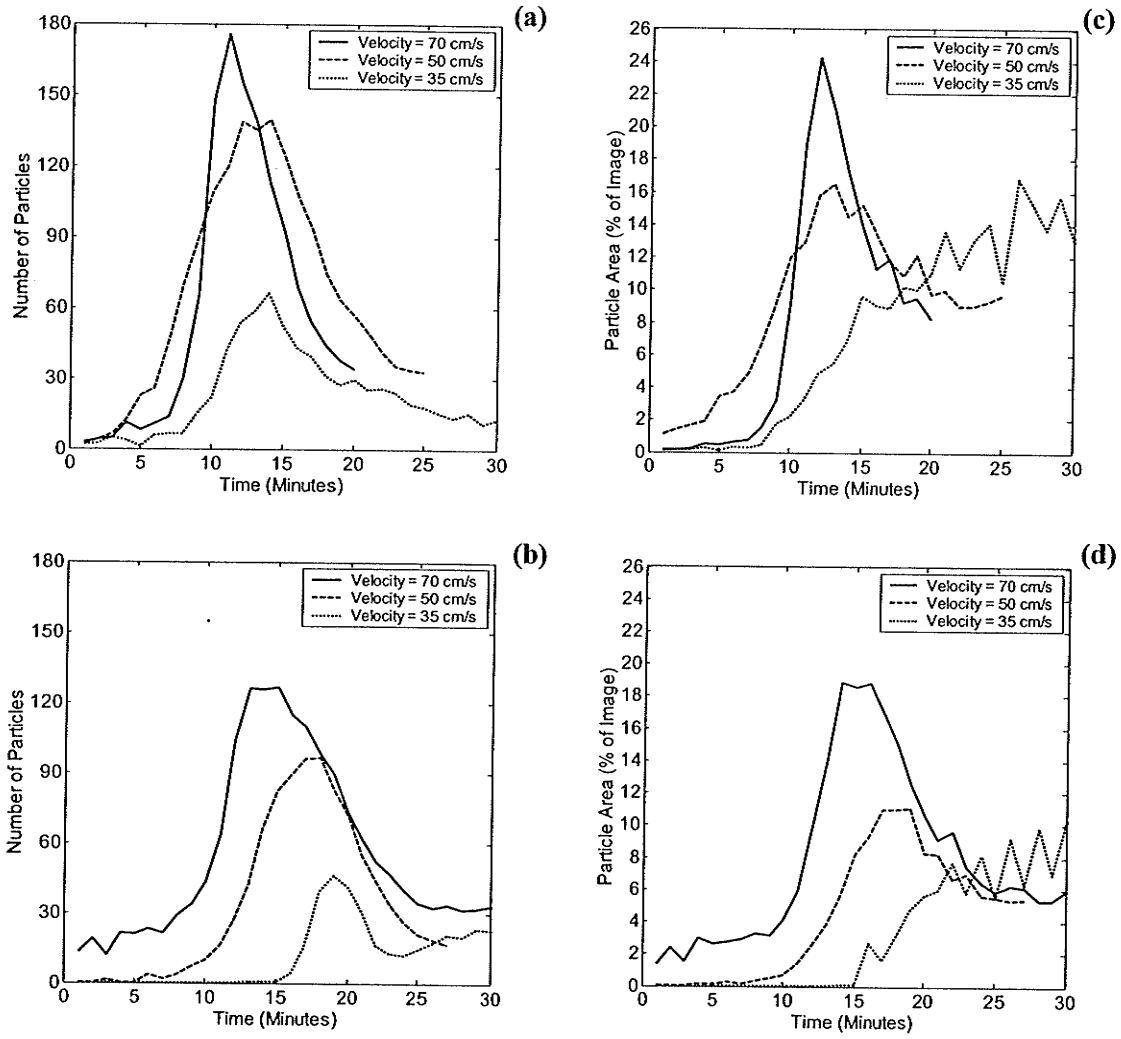

Figure 4.10. Time series of **(a)** the number of particles at temperature = -15°C, **(b)** the number of particles at temperature = -10°C, **(c)** the area of particles at temperature = -15°C, and **(d)** the area of particles at temperature = -10°C.

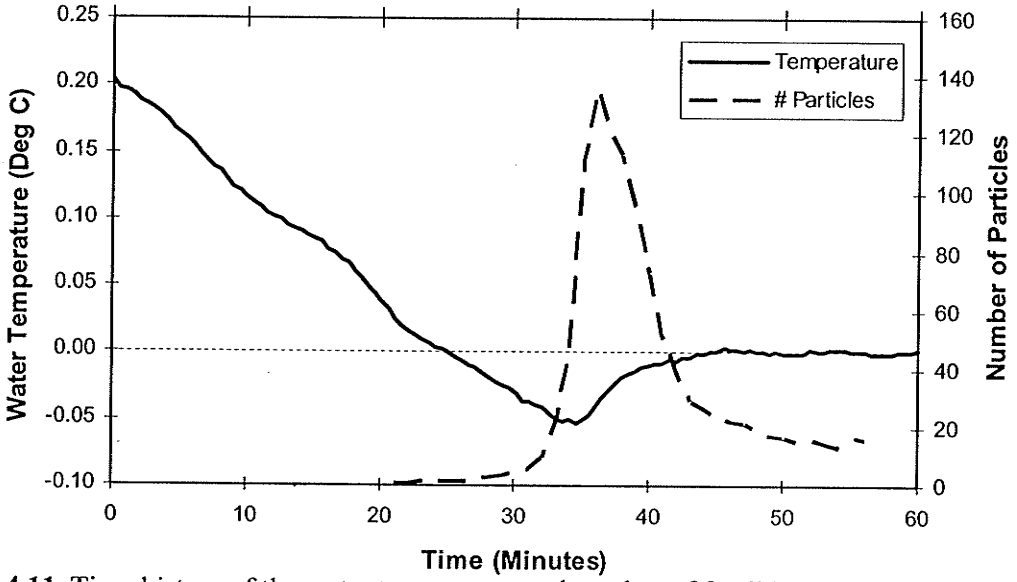

Figure 4.11. Time history of the water temperature and number of frazil ice particles.

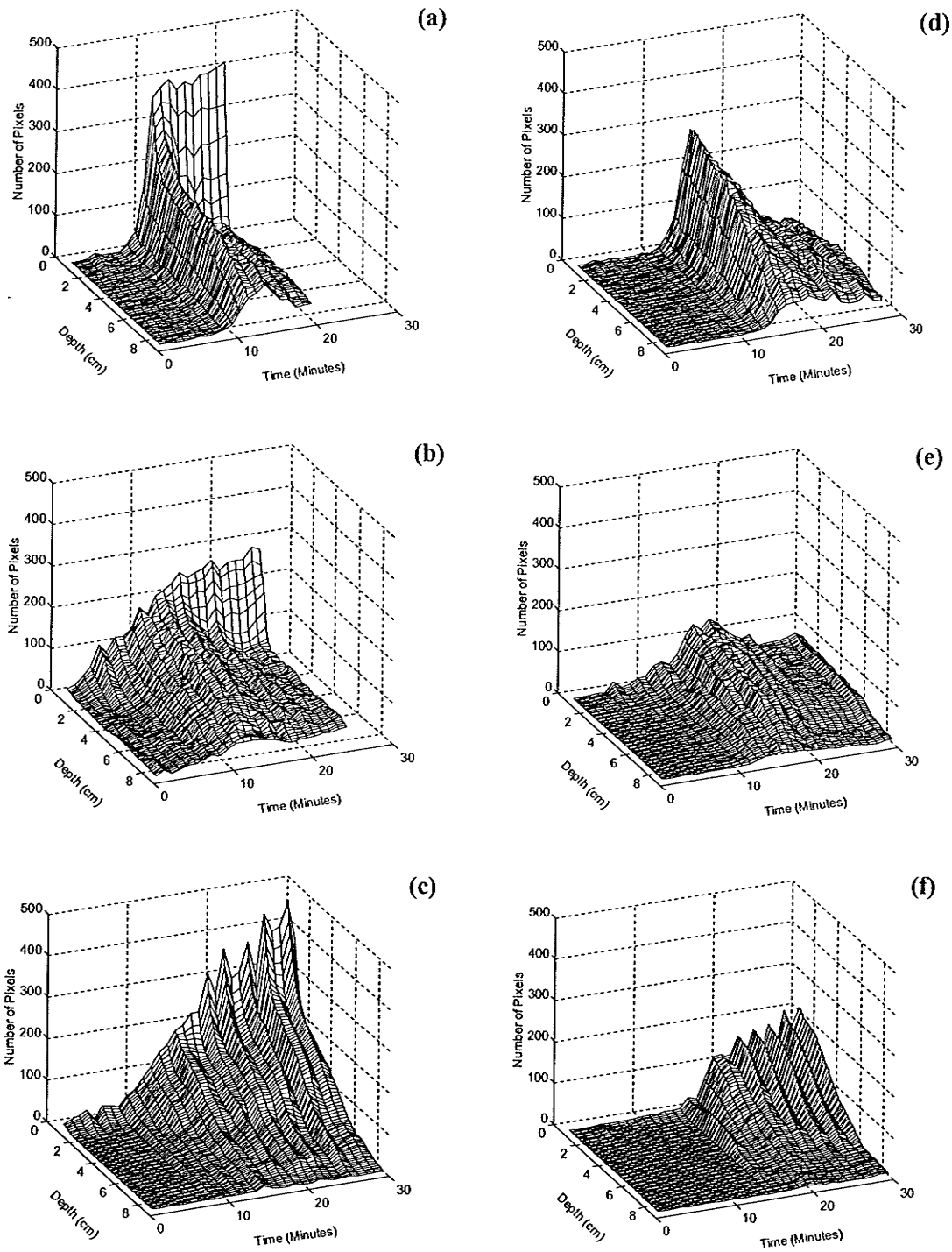

Figure 4.12. Time history of the vertical distribution of ice for **(a)** Run 1, **(b)** Run 2, **(c)** Run 3, **(d)** Run 4, **(e)** Run 5 and **(f)** Run 6.

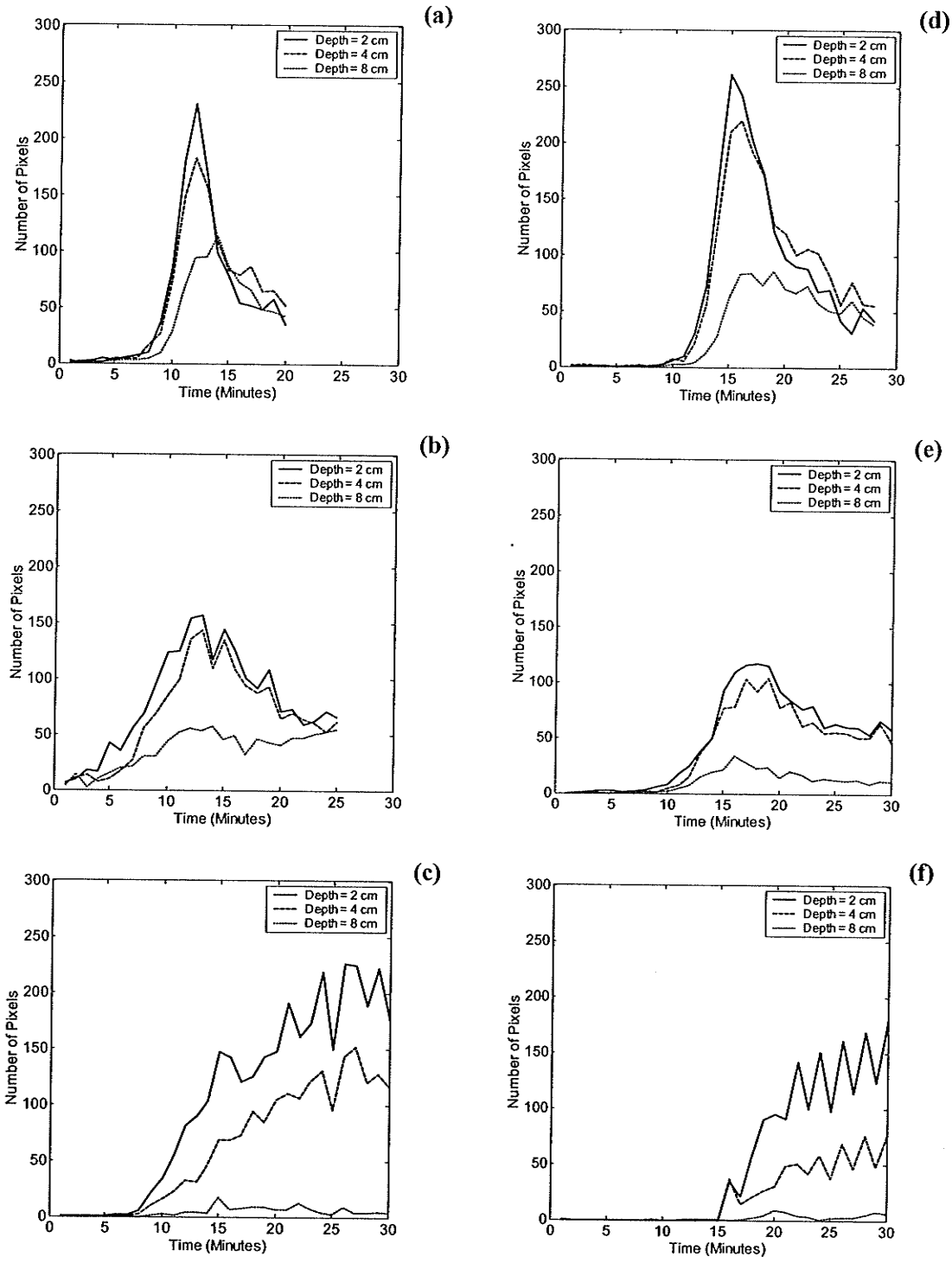

Figure 4.13. Vertical distribution history of ice at specific depths for **(a)** Run 1, **(b)** Run 2, **(c)** Run 3, **(d)** Run 4, **(e)** Run 5 and **(f)** Run 6.

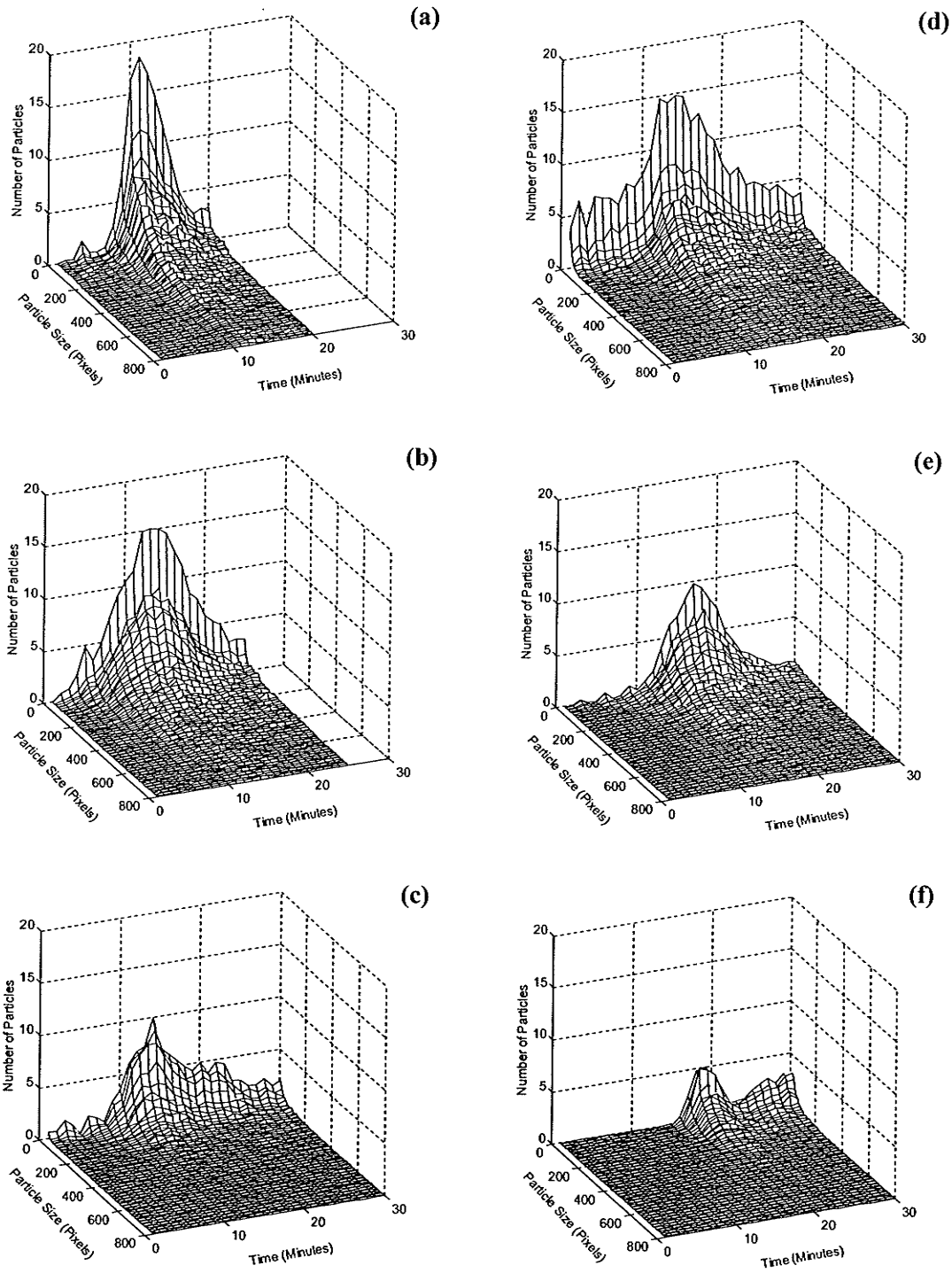

Figure 4.14. Particle size history for **(a)** Run 1, **(b)** Run 2, **(c)** Run 3, **(d)** Run 4, **(e)** Run 5 and **(f)** Run 6.

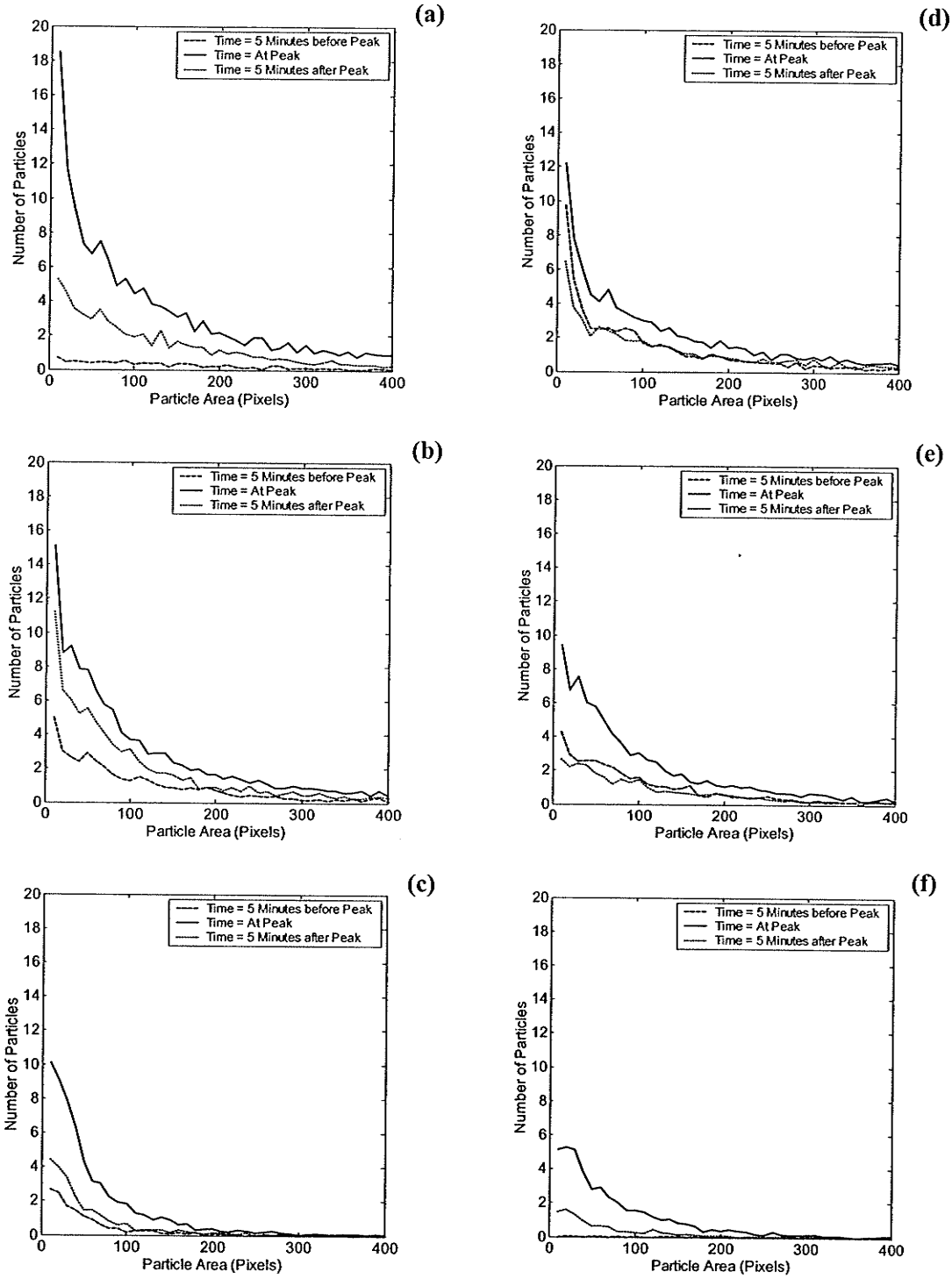

Figure 4.15. Particle size distribution at specific times for **(a)** Run 1, **(b)** Run 2, **(c)** Run 3, **(d)** Run 4, **(e)** Run 5 and **(f)** Run 6.

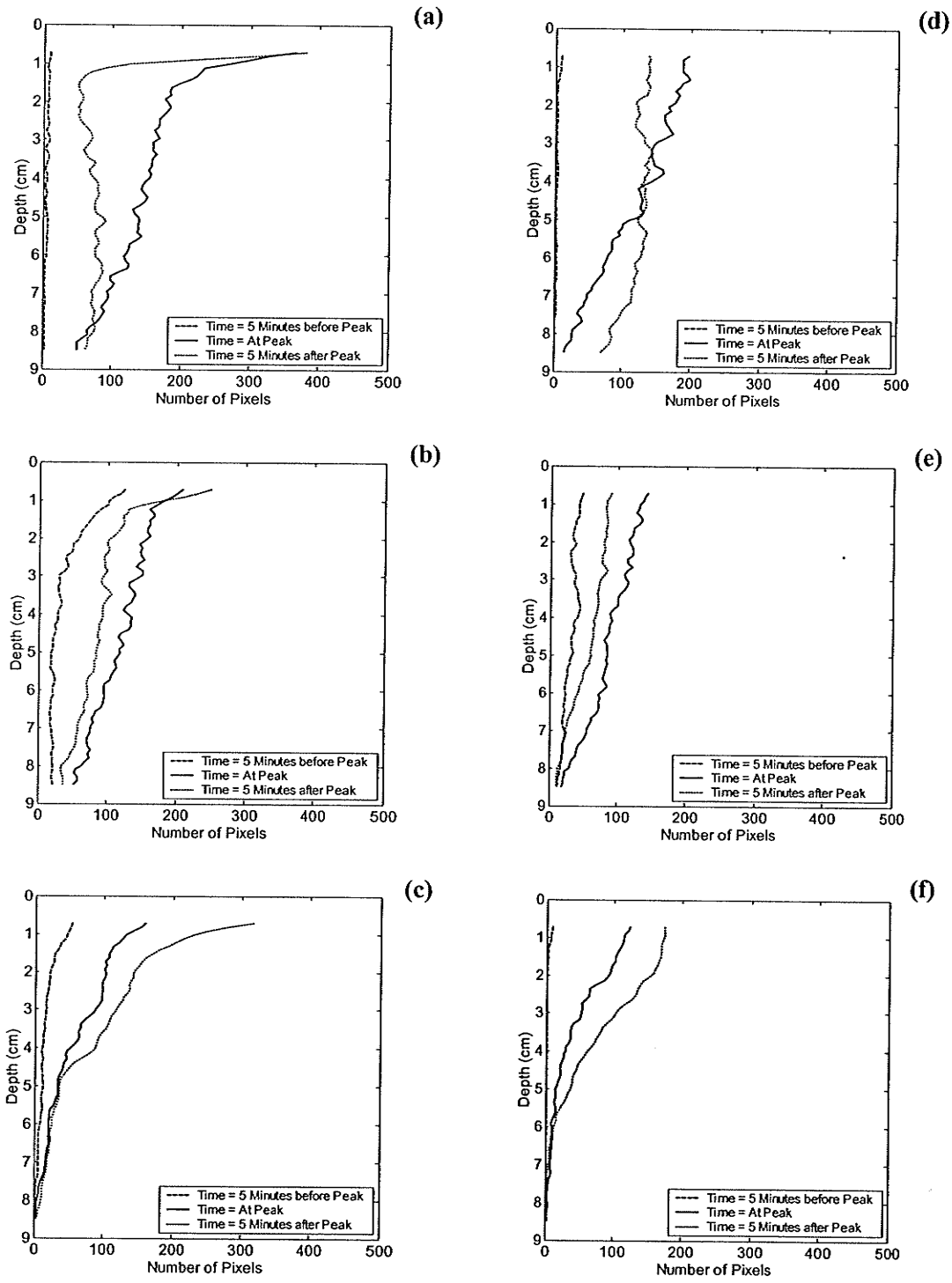

Figure 4.16. Vertical distribution of ice at specific times for **(a)** Run 1, **(b)** Run 2, **(c)** Run 3, **(d)** Run 4, **(e)** Run 5 and **(f)** Run 6.

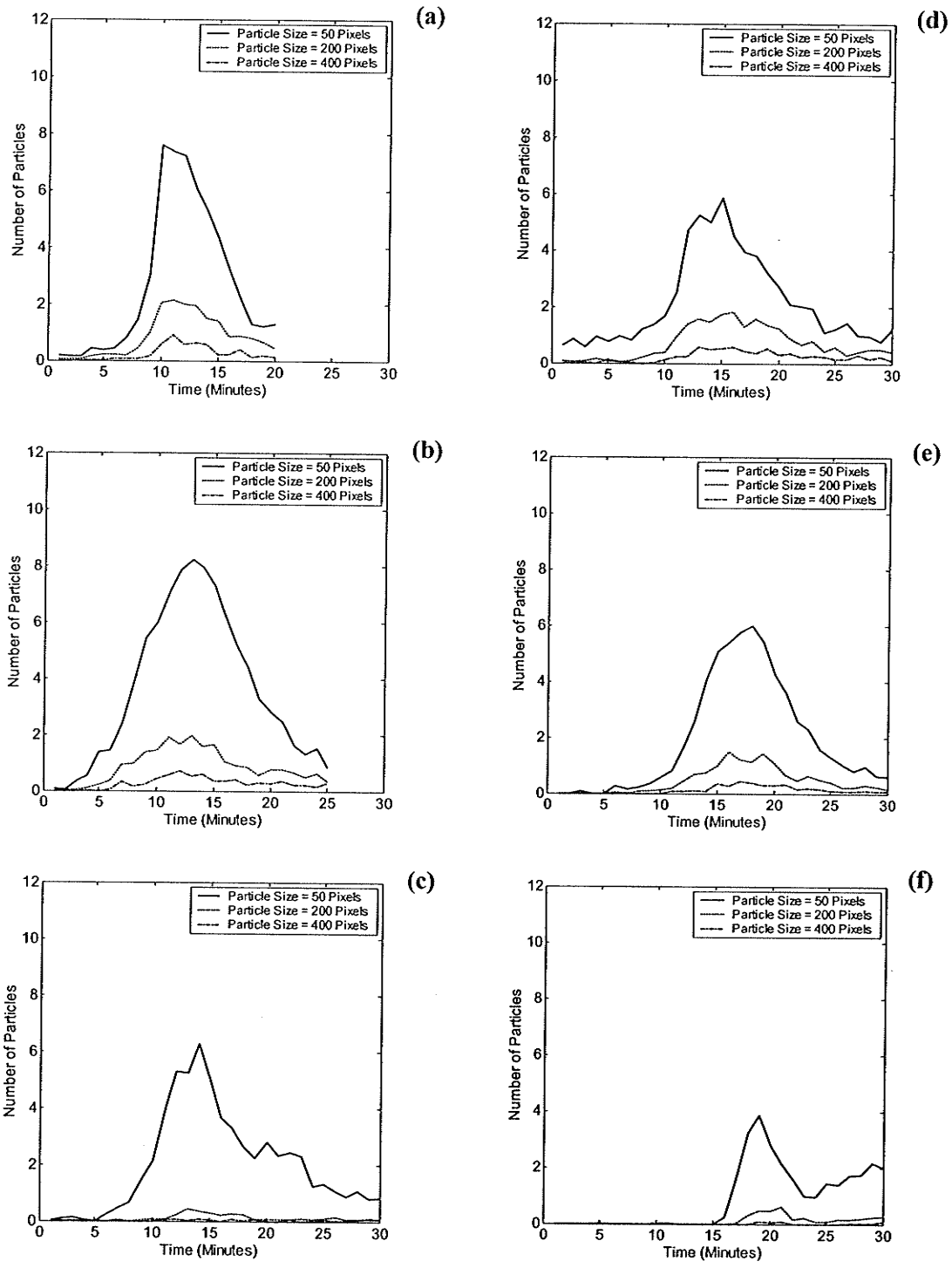

Figure 4.17. Particle size history for specific particle sizes for **(a)** Run 1, **(b)** Run 2, **(c)** Run 3, **(d)** Run 4, **(e)** Run 5 and **(f)** Run 6.

CHAPTER 5

Summary and Recommendations

5.1 Summary

Frazil ice has a significant economical and social impact in northern regions around the world. The ability to predict the evolution and behavior of frazil ice based on environmental conditions is an important step in minimizing its impacts on society. An important aspect of frazil ice research is the ability to accurately detect and measure frazil ice. A number of instruments have been developed that can indirectly measure frazil ice concentration using electrical conductivity, laser Doppler velocimetry, acoustics, calorimetry, or time-domain reflectometry. Although frazil ice concentration is an important characteristic, a more detailed feature necessary for the advancement of frazil ice research is the particle size distribution. Photography is an excellent method of obtaining this information. Successful attempts have been made at using photography to capture images of frazil ice. These images were then projected on an overhead screen and the visible frazil ice particles were manually counted. Due to the labour intensiveness of this manual approach, only a limited number of images were captured and analyzed. In an attempt to improve the speed of image analysis and collect larger quantities of data, a digital image processing system was developed herein.

Images of frazil ice are collected from a counter-rotating flume housed in a large cold-room, and stored on a computer. The images are then systematically analyzed to extract the number, size, and location in the water column of every particle. This system has the capability of analyzing thousands

of images per hour. The processing system is actually two separate programs, the image collection program and the image manipulation/analysis program.

The image collection program uses a camera, frame grabbing board and computer to collect a series of images. The images are collected in bursts, rather than continuously, to reduce the quantity of images accumulated. The images from each burst are first saved to the RAM of the computer, until all images from the burst have been collected. The images are then transferred to the hard drive. The images are collected using a cross-polarization light technique, allowing the normally transparent particles of ice to be distinctly detected.

After all the images have been collected for an experiment, the second program begins the analysis process. Images were analyzed by comparing the images with frazil ice particles (Ice Images) to images that do not contain ice (Reference Images). This removed all of the background noise leaving just the frazil ice particles. The images were then subjected to a series of morphological operations, in order to remove any noise elements and to create coherent frazil ice particles that could be easily counted and sized. The size and location in the water column of each frazil ice particle was recorded and stored in a manner that enabled the data from individual images to be recalled.

The digital image processing system was then used to analyze a series of experiments. The results indicated that the production of frazil ice in the flume and the subsequent analysis of the frazil ice images were very reproducible. The results of each experiment were also compared to reveal the effects of air temperature and water velocity on the water temperature and evolution of frazil ice.

From the analysis of the water temperature data, it was concluded that as the air temperature decreases, the cooling rate increases but the period of supercooling decreases. The data also indicated that higher cooling rates produced shorter periods of supercooling, but a larger degree of supercooling. All of the water temperature observations were consistent with previous frazil ice research conducted at other facilities.

The results of the particle analysis indicated that the peak number of particles observed in each experiment increased for cooler temperatures and higher velocities. The timing of this peak occurred sooner for cooler temperatures and higher velocities. For the lowest velocity experiments, a peak in particles was not observed; rather the number of particles seemed to slowly increase throughout the duration of the experiment.

The vertical distribution observations reveal that during the peak in ice particles, the concentration of ice decreased as the depth increased. As the experiment progressed, a few large flocs formed, dominating the water column. This phenomena was observed visually as well as through the image analysis. The concentration of ice at the lower depths also decreased considerable for the experiments conducted at the lower velocity due to the small levels of turbulence.

Definitive conclusions regarding the size distribution could not be reached due to the current limitations of the field of view of the cameras.

5.2 Recommendations

The University of Manitoba's counter-rotating flume is a one-of-a-kind piece of equipment that has the potential to make a valuable contribution to frazil ice research. With the development of the Digital Image Processing System (DIPS) described in this thesis, the flume may now be used to investigate the fundamental characteristics of frazil ice evolution. While working on the development of the DIPS, a few features were identified to further increase the value of future research.

The most important feature of digital image processing is the quality of the images to be analyzed. Higher quality images will yield higher quality data. One possible approach to increase the quality of the images captured on the counter-rotating flume is by improving the light source. Currently the flume uses two 23-Watt compact florescent light bulbs producing approximately 3000 lumens. By switching to a high efficiency metal halide light source with a reflecting shield, the amount of light could be increased by over 500% without the side effects associated with an enormous heat output.

The increased light output would improve the quality of the images in many ways. With more light, the shutter speed on the camera could be increased while reducing the aperture thereby improving the clarity of the ice particles. The increased brightness would also increase the contrast between the frazil ice particles and the surrounding water, decreasing the amount of noise. This may also identify particles that could not be seen under the lower light conditions.

Another way of increasing the quality of the images is to change the Plexiglas separating the water from the cameras. As the flume rotates, the Plexiglas flexes slightly. The magnitude of the flex is quite small and is impossible to detect to the naked eye. But under the cross-polarized light

conditions used on the flume, this small flex is very apparent and has an effect on the quality of the images collected. Removing the Plexiglas and replacing it with stiffer glass would eliminate the problems associated with the flexing. There are also other benefits of changing the Plexiglas. The scratches embedded on the Plexiglas are captured on every image used by the DIPS. Eliminating the scratches would eliminate the need to digitally remove them during image processing. Another major benefit would be the discontinuation of the LED apparatus. The purpose of the LED was to overcome the effects of the flexing Plexiglas. The removal of the LED system would eliminate a number of steps within the digital image processing system.

Another valuable aspect of frazil ice data collected from the flume is temperature data. The current temperature sensor and meter are not adequately stable or accurate. The thermometer has to be calibrated quite often in order to achieve the desired accuracy. A newer temperature-sensing device that is stable at all temperatures and accurate to within a few one-thousandths of a degree Celsius would prove to be an invaluable asset.

Currently the camera/lens combination used on the flume can detect a frazil ice particle with a diameter of approximately 0.6 to 0.8 mm. Increasing the light source and equipping the flume with some type of magnifying lens will drastically reduce the smallest detectable particle. Daly and Colbeck (1986) used a microscope/camera combination capable of detecting frazil ice particles as small as 30 microns.

If the flume is equipped with a magnifier then the quality of the water used in the experiments will have to be monitored. Any dirt particles suspended in water that are larger then the smallest detectable frazil ice particle will have to be removed. This will ensure that the dirt particles are not misinterpreted as frazil ice. Even if a microscope is not used, experiments should be performed to determine if the quantity of suspended particles affects the evolution of ice. The water used in the flume is taken from the City of Winnipeg's water supply, Shoal Lake. The quantity of suspended material varies from year to year and month to month. If the water quality affects the evolution of frazil ice in the flume, then steps should be taken to ensure the water quality is standardized for all testing.

Once all of theses issues have been dealt with, there is an exciting area of digital image processing to be explored. By adding multiple cameras, a 3D image can be created to examine an import aspect of frazil ice evolution, frazil shape. Currently the 2D images capture a projected image of the frazil ice

particles, revealing only the projected area. A 3D image would identify not only the size or volume of the particle, but the shape as well.

References

Ashton, G.D., (1986) River and Lake Ice Engineering, Water Resources Publications, Littleton, Colorado, 271-273.

Baxes, A.G., (1984) Digital Image Processing: A Practical Primer. Prentice-Hall, Englewood Cliffs, HJ, 169-170.

Burton, C.A., Johnston, L.J., and Sonenberg, E.A., (1995) An empirical investigation of thumbnail image recognition. http://www.ecr.mu.oz.au/~caburt/thesis7/node3.html (Accessed July 2000)

Carstens, T. (1966) Experiments with Supercooling and ice formation in Flowing Water. *Geofysiske Publikasjoner*, **26(9):** 1-17.

Daly, S. (1991) Frazil Ice Blockage of Intake Trash Racks. US Army Corps of Engineers Cold Regions Research Laboratory. Cold Regions Technical Digest No.91-1, March 1991.

Daly, S., and Colbeck, S.S. (1986) Frazil ice measurements in CRREL's flume facility. *Proc. IAHR Symposium on Ice*, Iowa City, vol. 1, 427-438.

Ettema, R., Karim, M.F. and Kennedy, J.F. (1984) Frazil Ice Formation. US Army Corps of Engineers Cold Regions Research Laboratory, Report 84-18.

Ford, J.S., and Madsen, N. (1986) Frazil ice record tests. *Proc. 4th Workshop on Hydraulics of River Ice, Montreal*, B3.1-B3.13.

Gilfilian, R.E., Kline, W.L., and Osterkamp, T.E., and Benson, C.S. (1972) Ice formation in a small Alaskan stream. UNESCO-5, Properties and Processes of River Lake and Ice.

Girling, W.C. and Groeneveld, J. (1999) Anchor ice formation below Limestone Generating Station, 10th workshop on ice, Winnipeg, Manitoba. 160-173.

Hammer, L. and Shen, H.T. (1994) Anchor ice growth and frazil accretion, IAHR ice Symposium Trondheim, 1059-1067.

Hanley, J., and Rao, S.R. (1981) Acoustic detector for frazil. Proc. IAHR Symposium on Ice, Quebec.

Hanley, T.O'D. and Michel, B. (1977) Laboratory formation of border ice and frazil slush. *Canadian Journal of Civil Engineering*, **4**: 153-160.

Jähne, B. (1993) Digital Image Processing: Concepts, Algorithms, and Scientific Applications, 2ed. Springer-Verlag New York. 253-259.

Kristinsson, B. (1970) Ice monitoring equipment. *Proc. IAHR Symposium on Ice, Reykjavik, Iceland*, 1970, 1-14.

Lever, J.H., Daly, S.F., Rand, J.H., Furey, D. (1992) A frazil ice concentration meter. Proc. *IAHR Symposium on Ice, Banff, Alberta*, 1362-1376.

MATLAB 2001. Using Matlab, Release 12. The Mathworks Inc., Natick, MA.

Michel, B. (1963) Theory of formation and deposit of frazil ice. *Proc. Annual Eastern Snow Conference, Quebec City, Quebec*, 130-148.

Osterkamp, T.E., Gilfilian, R.E., Gosnik, J.P. and Benson, C.S. (1983) Water temperature measurements in turbulent streams during periods of frazil-ice formation. *Annals of Glaciology*, **4**: 209-215.

Pegau, W.S., Paulson, C.A., and Zaneveld, J.R.V. (1996) Optical measurements of frazil concentration. *Cold Regions Science and Technology*, **24:** 341-353.

Schmidt, C.C., and Glover, J.R. (1975) A frazil ice concentration measuring system using a laser Doppler velocimeter. *Journal of Hydraulic Research*, **13**(3): 299-314.

Shen, H.T. (1996) River ice process-State of Research, *IAHR Proceedings of The 13th International Symposium on Ice*, Beijing, China, Aug. 27-31, Vol.3, 825-833.

Tsang, G., (1985) An instrument for measuring frazil ice concentration. *Cold Regions Science and Technology*, **10**: 235-249.

Tsang, G., and Hanley, T.O'D. (1985) Frazil formation in Water of different salinities and supercoolings. *Journal of Glaciology*, **31(108):**74-85.

White, K.D. and Daly, S.F. (1994) Experimental investigation of frazil ice in International Association for Hydraulics Research, Working Group on Thermal Regimes, Report on Frazil Ice, S. Daly, Editor. *USACE Cold Regions Research & Engineering Laboratory Special Report* 94-23: 5-10.

Yamazaki, M., Hirayama, K., Sakai, S., Sasamoto, M., Kiyohara, M., Takiguchi, H. (1996) Formation of frazil and anchor ice. *IAHR Proceedings of The 13th International Symposium on Ice*, Beijing, China, Aug. 27-31, Vol.2, 488-496.

Yankielun, N.E., and Gagnon, J.J. (1999) Laboratory tests of a time-domain reflectometry system for frazil ice detection. *Canadian Journal of Civil Engineering*, **26**: 168-176.